Exploring transferability of plastic-water hyacinth interaction and detection in rivers

Giel W.A. Hagenbeek[1,2,*], Tim H.M. van Emmerik[2,**], Tianlong Jia[3,4], Pummarin Khamdahsag[5], Kittiphon Boonma[6], Riccardo Taormina[3], Thomas Mani[7], and Marc Rußwurm[1,8]

[1]Geo-information Science and Remote Sensing Laboratory, Wageningen University and research, Droevendaalsesteeg 3, Wageningen Gelderland 6708 PB, the Netherlands
[2]Hydrology and Environmental Hydraulics Group, Wageningen University and research, Droevendaalsesteeg 3, Wageningen Gelderland 6708 PB, the Netherlands
[3]Delft University of Technology, Faculty of Civil Engineering and Geosciences, Department of Water Management, Stevinweg 1, 2628 CN Delft, The Netherlands
[4]Karlsruhe Institute of Technology (KIT), Institute of Water and Environment, Karlsruhe, Germany
[5]Sustainable Environment Research Institute, Chulalongkorn University, Bangkok 10330, Thailand
[6]Geoinformatics Center, Asian Institute of Technology, Pathumthani, Thailand
[7]The Ocean Cleanup, Rotterdam, the Netherlands
[8]University of Bonn, Institute for Food and Resource Economics, Bonn, Germany
[*]Correspondence: giel.hagenbeek@wur.nl
[**]Correspondence: tim.vanemmerik@wur.nl

SUMMARY

Rivers are major pathways for plastic pollution to oceans, with high emissions in tropical regions. Research in the Saigon River showed that invasive water hyacinths (WHs) can trap macroplastics and serve as proxies for detecting river plastic using remote sensing. We explore this phenomenon and its detection methods transferability to the Chao Phraya River. Along a 62.1 km river course, WHs trapped an average of 32% of floating plastics, reaching local maxima of 78%, comparable to 58–82% in the Saigon. Plastic concentration in WHs was 59 times higher than in open water, increasing downstream. Object detection models transferred well for WHs and entangled plastics (Chao Phraya: mAP_{50} = 68% and 54%; Saigon River: mAP_{50} = 70% and 52%), but poorly for free-floating plastics (23% vs. 48%). Physical sampling found 14 times more plastics within WHs than imagery, highlighting WHs' role in trapping plastics and their potential for monitoring and targeted clean-up efforts.

KEYWORDS

plastics, pollution, rivers, object detection, remote sensing, hyacinths

INTRODUCTION

Marine, freshwater and terrestrial environments are increasingly polluted with plastic waste. This widespread pollution threatens ecosystems, biodiversity, human health, livelihoods, and economic productivity[1]. Rivers play a significant role in transporting land-based plastics towards the oceans, with annual river plastic emissions estimated to range from 0.8 to 2.7 million tons[2]. To support plastic pollution reduction and prevention strategies, monitoring of plastic pollution is

crucial[3–5]. The United Nations Environment Program (UNEP), in its draft legally binding instrument on plastic pollution, emphasizes the importance of identifying plastic hotspots in developing reduction strategies[6]. Satellite remote sensing (RS) is a relevant method for upscaling measurements and has shown the potential to monitor macroplastics in marine environments[7–11]. However, the spatial resolution of RS imagery is often too low for plastic debris detection, limiting its use to large plastic patches and items, leading to an underestimation of total plastic debris[12–15]. Therefore, in-situation data collection is required for plastic detection, making coverage of large areas difficult due to the labor, costs and time involved[16]. To successfully monitor riverine macroplastics from space, debris patterns, such as vegetation and wood, are being explored as detectable indicators[12,17].

Tropical and subtropical rivers dominate global riverine plastic emissions[2,18,19]. In addition, tropical rivers are increasingly infested with water hyacinths (WHs), *Pontederia crassipes* (formerly *Eichhornia crassipes*).

This free-floating weed, with fast growth, reproducibility and light-blocking mat-like clustering, is regarded as one of the most invasive aquatic weeds worldwide, and ways to monitor and eradicate them are actively sought[20,21]. At the same time, WHs have been shown to trap or entangle debris, such as plastics. Research in the Saigon River, Vietnam found that of all floating plastics, between 54% and 78% at specific cross-sections, and up to 73% over a 42 km spatial extent were trapped in WHs[22–24]. RS using Sentinel-2 satellite imagery has shown to be successful in detecting WH patches in freshwater bodies, including tropical rivers[25,26]. Given that 1) WHs can be detected with RS and 2) WHs act as a plastic-trapping mechanism, WH coverage can be used as a proxy for detecting plastics from space[23,27,28].

Beyond the Saigon River, anecdotal evidence of the co-occurrence of plastics and WHs has been reported in other tropical rivers like the Ozama River in the Dominican Republic, the Citarum in Indonesia, the Vam Co Dong River in Vietnam and Chao Phraya River in Thailand.[12,29,30]. To use WHs as a generally applicable proxy indicator for macroplastics in rivers, its transferability to other river systems needs to be assessed[23]. The found relationship between plastics and WHs over the Saigon Rivers' spatial extent supports the potential transferability of this phenomenon to other hyacinth-invaded fluvial systems[24,31]. However, the drivers of plastic transport dynamics in rivers, especially in complex areas such as confluences and tidal regimes, remain poorly understood, creating uncertainties in plastic transport estimates and scaling efforts[30,32]. Although the primary factors driving macroplastic transport are not fully understood, WHs can facilitate this transport either through their trapping mechanisms, by exhibiting dynamics similar to those of plastics, or simply by coinciding spatially with them[23]. Understanding these interactions in different fluvial systems is therefore essential when using WHs as a proxy for plastic pollution.

Previous assessments used two main modules to investigate plastic-hyacinth interactions. First, a Sentinel-2 approach using a Naive-Bayes classifier was used to detect WHs in the Saigon River. While this automated classification approach is assumed to be transferable to other river systems, the classifications' true applicability remains uncertain, particularly due to challenges such as cloud cover, WH patch sizes and seasonal variability[25]. Second, to investigate plastic-hyacinth metrics such as trapping ratio and plastic concentration within WHs, in-situ data collection of Uncrewed Aerial Vehicle (UAV) imagery and fixed cameras were used to collect input for deep learning object detection using You Only Look Once v8 (YOLOv8)[33]. The model was trained on data for the Saigon river, although the application of this approach to another river system remains unknown[24]. This aligns with a broader knowledge gap regarding the generalization performance of deep learning models to detect macroplastic litter in varying geographical and environmental conditions[34]. This paper has three specific goals. First, we aim to evaluate how Sentinel-2 WH detection is applicable as a valid and useful method when applied to a different river system. Second, we aim to define detection model transferability for plastics

and WHs in on-site imagery. Lastly, we aim to determine whether plastic-hyacinth interactions are specific for the Saigon, or whether this phenomenon can serve as a reliable proxy for riverine macroplastic pollution in a different geographic and hydrological context, the Chao Phraya River in this case. With this paper, we assess the transferability of plastic-water hyacinth interactions, and field-based and remote sensing detection methods.

METHODS

Sentinel-2 imagery was used to retrieve WH coverage. In-situ imagery from UAVs and bridge-mounted cameras served as input for object detection of plastics and WHs, allowing comparison with satellite-derived WH estimates. Visual plastic counting and physical sampling was performed to validate plastic density and support the interpretation of object detection results.

Study area

The Chao Phraya River is approximately 372 km long and flows from northern Thailand through Bangkok before discharging into the Gulf of Thailand[35]. With its basin of approximately 158,000 km^2, it is the fifth largest basin in Southeast Asia. The basin accounts for 30% of Thailand's surface area, making it one of the most important resources for irrigation, transportation and fishery of the country[36]. Within the Bangkok Metropolitan Area, discharge averages around 700 m^3s^{-1}, and peaks up to 6,000 m^3s^{-1}[37]. The river's discharge is highly influenced by the tropical monsoon climate, resulting in three distinct seasons: hot (Feb–May), rainy (May–Oct) and dry (Oct–Feb). The lower Chao Phraya discharge is further influenced by tides, leading to fluctuations in discharge of up to $\pm$3000 m^3s^{-1}. Tidal ranges can exceed 3 m and tidal intrusion reaches up to 175 km upstream during low flow periods and up to 75 km during high stream flow periods[38,39].

Satellite remote sensing data

Sentinel-2 imagery offers high-resolution multispectral data (10–20 m depending on the band), covering red-edge, near-infrared (NIR), and shortwave infrared (SWIR) bands, which are well-suited for detecting floating vegetation due to their distinct spectral signatures[25]. Atmospherically Sen2Cor[40]-corrected 12-band Sentinel-2 L2A scenes were retrieved from SentinelHub, covering the entire study area from 1 June 2024, to 1 June 2025, including a 5 km buffer at both the northern and southern river extents. A total of eight tiles were used to retrieve the scenes, equally divided across the four river segments shown in Figure 1. Scenes with cloud coverage above 80% were not used. Only dates with scenes available across all river segments were used, resulting in 27 scenes per segment for full-year analysis and 5 scenes per segment aligned with the fieldwork period.

To estimate WH coverage, we used a Naive Bayes–based classifier, which was trained on hand-annotated 10 × 10 m Sentinel-2 pixels (n = 600) from the Saigon River using the *scikit-learn*[41] Python package with an 80:20 training–testing split by Janssens et al.[25]. Training and test sets were based on visual selection of reflectance values of Sentinel-2 bands, Normalized Difference Vegetation Index (NDVI) and Floating Algae Index (FAI). Figure S1 illustrates the spectral reflectance and index-based differences between WHs and open water derived from this dataset, including NDVI and FAI values, demonstrating the separability used to train the classifier.

The model was implemented in Google Colab using the *eo-learn*[42] collection of Python packages. We applied the model as provided, without retraining on new data from the Chao Phraya River.

The classifier inputs 5 features, i.e., NDVI, FAI[43], and the blue (B2), green (B2) and shortwave infra-red bands (B12) and estimates the likelihood of hyacinth presence. After cloudmasking using Python package *S2cloudless*[44], the remaining pixels were categorized by the built-in Scene Classification Layer (SCL) with water (SCL=6), bare soil (SCL=5), or vegetation (SCL=4). A total of 2006 hectares of river surface over 79 km of river was used, divided into four segments to align with the distribution of in-situ data collection: upstream (678 ha), upper midstream (405 ha), lower midstream (451 ha), and downstream (472 ha) (Figure 1). The output of the model yields the coverage of WHs as percentage of the river (section) area.

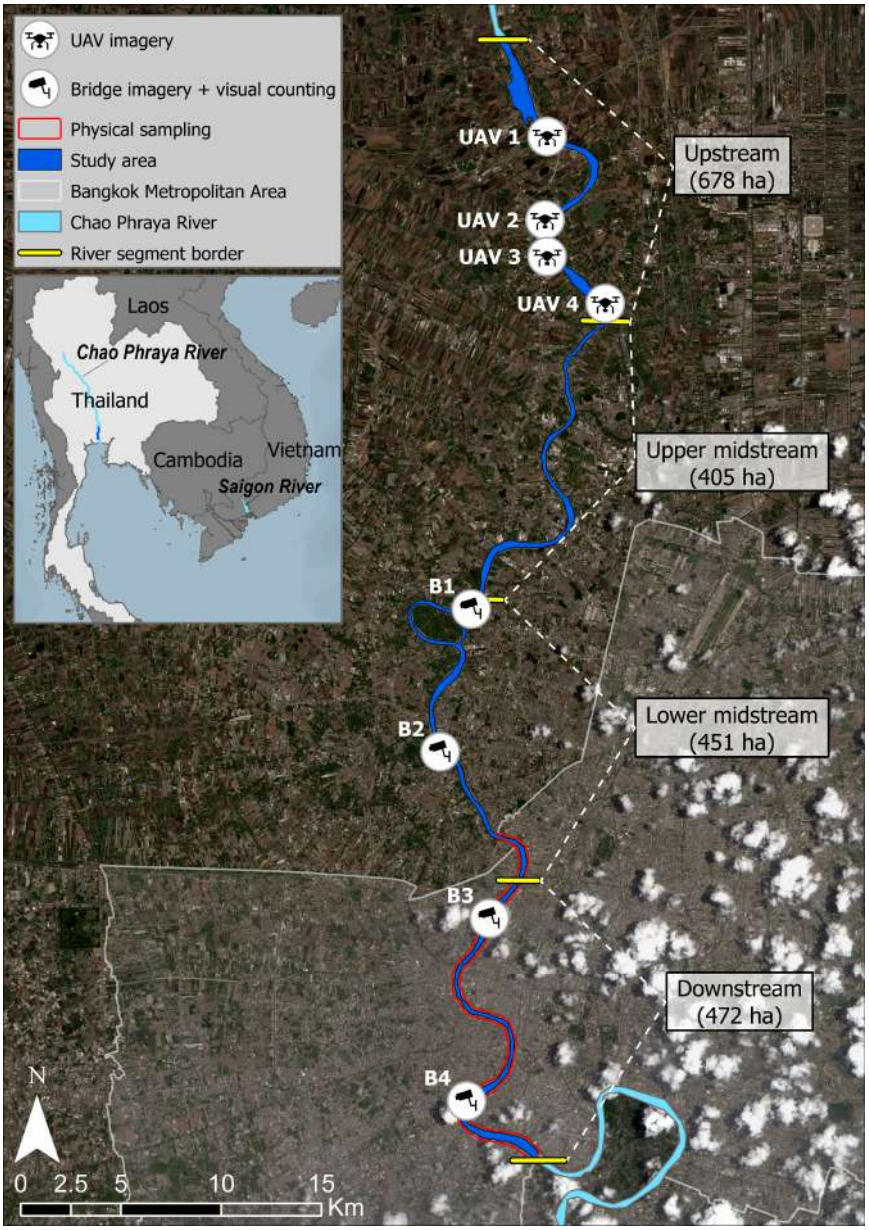

Figure 1: Study area and location of in-situ data collection locations, with an RGB (red, green, and blue) Sentinel-2 scene from April 25, 2025 as basemap.

Field data collection

Measurements were performed during the dry season, between 17 March and 26 April 2025. Four data collection methods were used: (1) the collection of bridge-mounted camera imagery, (2) UAV imagery, (3) visual counting, and (4) physical sampling of WH patches. All measurements were spread over a 62.1 km length of the river, with the most northern part 104.5 km upstream of the Gulf of Thailand and the most southern part 42.4 km away.

Bridge-mounted camera imagery

Four bridge locations were revisited during four periods, during which a single GoPro Hero 11 (GoPro, Inc., San Mateo, USA) was deployed on one bridge per day in a fixed order (B1–B4). At B1 the GoPro was deployed on the South side to avoid capturing a ferry and on B2-B4 on the North side. The GoPro was mounted on a 1 m arm to capture nadir images without including bridge structures (Figure 2a,c). Images were taken using the 8:7 linear lens. Per bridge, five waypoints were equally distributed across the width of the river, to capture characteristics over the full width of the river.Waypoint spacing prevented image overlap at all bridge.. The Field of View (FOV) at the outer waypoints was set to cover the river surface only, avoiding the riverbank and overhanging structures, such as piers or buildings. All waypoints were revisited in six rounds per date, evenly split between morning and afternoon, except B3 in period three (Table 1). Each round proceeded west to east. The GoPro was set to take an image every 10 seconds, during a span of 5 minutes per waypoint, planned to yield 31 images per round per waypoint. The final amount of images captured per waypoint and round was influenced by battery level, camera-overheating and manual mistakes. In total 14,742 images were taken and used without further filtering (Table 1). Camera height at waypoints 1 and 5 was measured using a MK202 distance laser reflecting off the riverbank at water level, as direct measurements from the water surface were not possible due to low reflectivity. Distances were recorded once at high tide and once at low tide. Bridge center height was estimated from the bridge structure elevation, and for waypoints 2 and 4 the average of the outer and middle waypoints was used. Camera height of each individual image were taken into account, and used as input for the calculation of the ground sampling distance (GSD), which we elaborate on in the 'imagery-processing' section.

UAV imagery

On 20 March and 4 April, UAV images were collected at four river cross-sections, at locations different from the bridge-mounted imagery, as shown in Figure 1. Each location was revisited in the morning and afternoon for equal distribution between tides (except for UAV4, on the 20th of march, which was only visited in the afternoon). A DJI Mavic 3 Enterprise (SZ DJI Technology Co., Ltd., Shenzhen, China) with RGB camera, a 4/3 CMOS sensor and 20 megapixels was used. UAV flights were performed by a parallel flying pattern[45], crossing the river perpendicularly to the water flow, as shown in Figure 2b. Per location, the UAV crossed the river between 38 and 70 times spread over two periods (Table 1). The number of river crossings per location varied due to battery levels, as time did not allow for recharging after every flight. Flight height and river width influenced the time required per crossing, further constraining consistency. Flight height was aimed to average 10 m for optimal performance[46], with deviations caused by surrounding conditions at the take-off location. To limit capturing the same flowing hyacinths, each returning river crossing moved slightly further against the direction of the river flow. Parallels were not aimed to be overlapping. Images were taken at a constant interval while flying from riverbank to riverbank. A total of 9,884 images were taken. Images of the riverbank were filtered out manually (n = 3,482). All other UAV images were used (n = 6,402) (Table 2).

Table 1: Details per bridge and UAV locations, including rounds of observations per period. Distance to the Gulf of Thailand was measured along the river centerline, following the channel. The meander cutoff under location B1 was included in the total distance, whereas the longer meander loop was not.

Location ID	Lat	Lon	km upstream	River width [m]	Rounds per period			
					17–21 Mar	24–28 Mar	8–12 Apr	22–26 Apr
UAV 1	14.12086	100.5265	104.5	300	33	-	37	-
UAV 2	14.08607	100.5254	97.8	390	23	-	15	-
UAV 3	14.06883	100.5274	95.3	227	37	-	27	-
UAV 4	14.04866	100.5533	92.2	247	10	-	26	-
B1	13.91570	100.4939	72.4	191	6	6	6	6
B2	13.85368	100.4803	64.6	280	6	6	6	6
B3	13.78107	100.5024	54.3	333	6	6	7	6
B4	13.70090	100.4921	42.4	375	6	6	6	6

Table 2: Camera setup and image statistics for each location

Location ID	Camera height [m]			GSD [cm/pixel]		FOV [m^2]		# Images after filtering	Annotated Images	Annotated Items
	min	max	avg	min	max	min	max			
UAV 1	4.59	19.18	10.82	0.12	0.51	31	545	2246	9	104
UAV 2	9.26	14.39	11.16	0.25	0.38	127	307	1592	7	242
UAV 3	10.03	17.62	11.73	0.27	0.47	149	460	1688	10	47
UAV 4	9.46	12.83	11.11	0.25	0.34	133	244	876	9	136
UAV total								6402	35	529
B1	11.10	12.00	11.46	0.46	0.50	574	671	3874	17	426
B2	10.40	12.40	11.20	0.43	0.51	114	717	3592	10	50
B3	5.50	6.50	5.90	0.23	0.27	132	197	3614	10	71
B4	6.20	10.70	8.00	0.26	0.44	156	534	3662	10	339
Bridge total								14742	47	886
Total								21144	82	1415

Visual counting of floating plastic

Visual counting was performed at each waypoint, nearly simultaneously with bridge imagery. Over the span of 5 minutes, all litter flowing into the visual FOV was counted. Debris already present in the FOV before counting began, whether stationary or exiting, was not counted. The visual FOV is different from the bridge-mounted camera FOV, with a constant width estimated at 15 m. When plastic flow was too fast to count ($>$27,000 items h^{-1}), the number was estimated by groups of 10 or counting durations was reduced to less than 5 minutes (n = 26). The minutes of counting was noted per observation. For each counted item it was noted whether it was free-floating or entangled in WHs (Figure 2c). Additionally, all litter was assigned to its corresponding plastic category (Table S2), based on the common plastic type classifications of the item, as seen from the bridge[27,30]. We used 8 distinct groups for plastic categorization: polyethylene terephthalate (PET), soft polyolefin (POsoft), hard polyolefin (POhard), multilayer plastics (ML), polystyrene (PS), expanded polystyrene (EPS), other plastics, rubbers and other litter. The categories POhard and POsoft encompass both polyethylene (PE) and polypropylene (PP). During high plastic flow events, categorization took place for 1 minute following an extrapolation to the total plastics counted in the total counted minutes. A total of 13,491 items were classified, of

which 13,355 being polymers and rubbers. Other litter (n = 136) is not further taken into account in the analysis. From here on, plastics will refer to both polymers and rubbers. From the visual counting observations, the surface plastic transport rate [#/h] was estimated following Schreyers et al.[23], by normalizing plastic counts by observation time and scaling by river width. Trapping ratio [-] was retrieved by dividing the summed counted entangled plastics by the summed total plastics per waypoint per round. Hereafter, the trapping ratio was averaged across waypoints and rounds to get a representative value for the river width per date and location.

Physical sampling

Physical sampling of WH patches was conducted over four consecutive days, from 1 to 4 April, between 08:30 and 15:00 (UTC+7) each day. The sampling took place working together with the river cleaning team of the Bangkok Metropolitan Administration (BMA) and within their perimeter, the Bangkok Metropolitan Area, as outlined in Figure 1. A team of 2–3 people collected WH patches from a boat using round dip nets, which are ordinarily used by the BMA for litter collection, as shown in Figure 2d. The nets were submerged directly in front of the patches to minimize the simultaneous collection of entangled and free-floating debris. After extraction, all caught material was placed into a basket, after which WH was separated from anthropogenic debris. The wet mass per WH patch was measured on board using a scale. In some cases (n = 8), multiple small patches were combined and weighed together, and the anthropogenic debris was sorted collectively. On board, all plastics were sorted and counted according to the categories described in the Visual Counting section. Only plastics $\geq$ 0.5 cm in any dimension were included.

All collected plastics were preserved for subsequent mass analysis on shore. A representative quarter of the total number of items was then selected, categorized, and weighed to calculate the mean mass per plastic type (kg). Plastic concentrations per WH were recorded as 1) plastic area concentration [# items/ m²], and plastic mass concentration [g/kg]. In total, 58 patches were sampled, together making up for approximately 200 kg of wet biomass. A total of 1,832 plastic items were found, making up for 5 kg in total. The estimated surface area of individual samples ranged from 0.03 to 2.25 m², with an average of 0.57 m², totaling 25 m² across all sampled WHs.

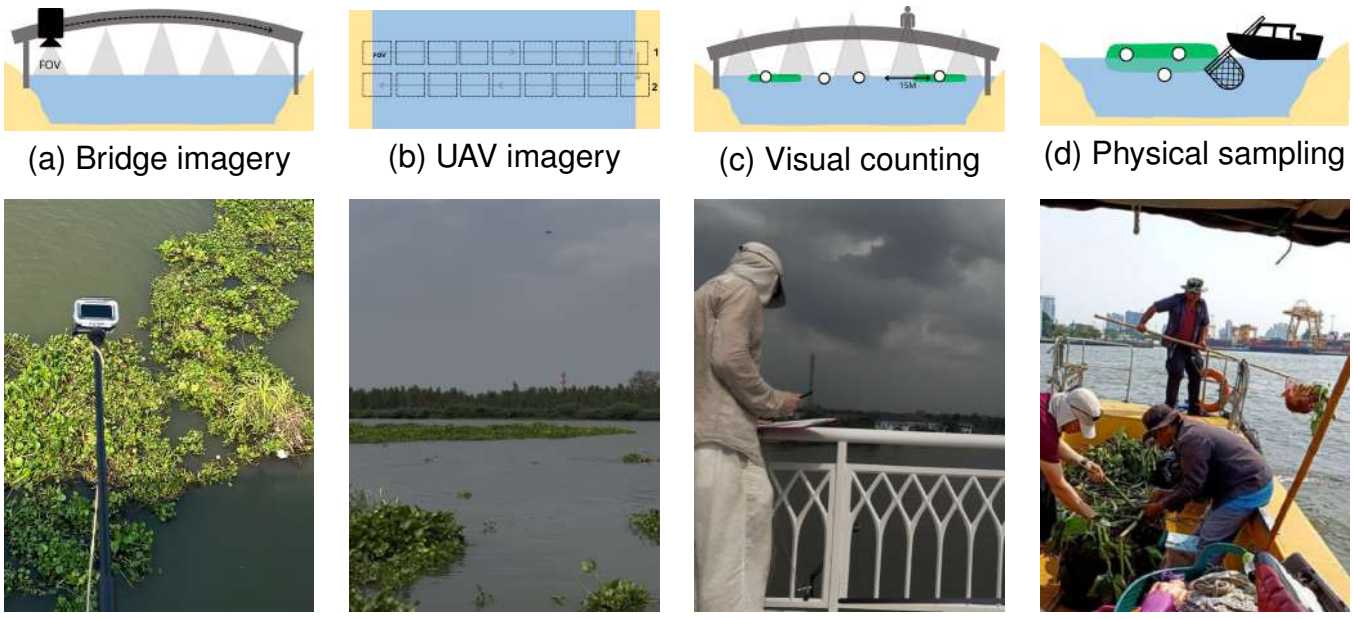

(a) Bridge imagery (b) UAV imagery (c) Visual counting (d) Physical sampling

Figure 2: Overview of data collection methods. Top row shows methodological approaches (a–d), with representative field photographs shown below each method.

Imagery processing

This section describes the imagery processing using the object detection model applied to bridge-mounted camera and UAV imagery.

Model description

YOLOv8 deep learning architecture[33] was used to detect WHs and plastics in all UAV and bridge imagery. YOLOv8 is a one-stage convolutional neural network for real-time object detection. It has two main parts: a backbone that extracts multi-scale features by balancing depth, width, and resolution, and a detection head that detects objects and outputs bounding boxes to show the object type and location.

Two models developed on Saigon River imagery were applied directly to the Chao Phraya River, without any retraining. Due to YOLOv8's input size limitation (maximum 640 × 640 pixels), these models were originally developed using two separate imagery processing methods. The HyacinthModel was trained on resized images (n = 218) and (2) the PlasticModel was trained on tiled images (n = 11,408)[24]. Both models are trained on three classes: 1) WHs, 2) free-floating plastic, and 3) plastic entangled in WHs[47]. The PlasticModel was used to retrieve both free-floating and entangled plastic counts from tiled images. The HyacinthModel was used to retrieve WHs from the resized images. Tiling cut an original image into 56 (GoPro) or 48 (UAV). Resizing takes the original image and reduces it to image size 640 by 640 pixels. All UAV and bridge imagery was used as input for both models, after which all detections were matched back to the original image for integrated analysis, as visualized in Figure 3.

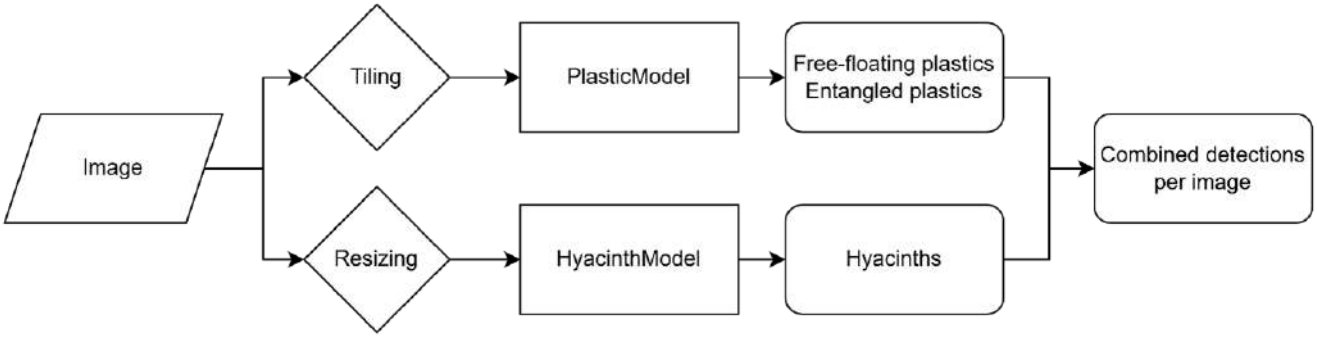

Figure 3: Visual representation of the framework used to retrieve final metrics per image.

Model performance evaluation

To evaluate the model performance on the Chao Phraya River a validation set of 82 images was created out of a total of 21,144 images (70% GoPro, 30% UAV). A total of 1,415 objects were annotated using LabelStudio[48] (54% GoPro, 46% UAV), used for the HyacinthModel. Additionally, these annotations were cut into tiles to align with the tiled images, which may have excluded objects partially outside tile boundaries, resulting in 1,346 annotations for the PlasticModel. The number of annotated items per class was kept approximately equal (Table S3). For both models, the bounding box coordinates were recalculated to the original image size.

Model performance was evaluated on a hand-annotated validation set using commonly used YOLOv8 metrics[34,49,50]: 1) precision, the ratio of correct detections to total detections; 2) recall, the ratio of correct detections to actual objects; 3) mAP50, the mean average precision at an Intersection over Union (IoU) threshold of 0.50; and 4) mAP50–95, the mean average precision

averaged across IoU thresholds from 0.50 to 0.95. The model performance evaluation was run with a default confidence threshold of 0.5.

Model output settings

To determine suitable confidence scores for running the two models, validation set predictions were evaluated against ground truth annotations. IoU was used to determine matches between predicted and ground truth bounding boxes. A detection was counted as a True Positive (TP) if the IoU was ≥ 0.5 and the predicted and ground truth class labels matched. Predictions without matching ground truth were counted as False Positives (FP), and unmatched ground truth boxes as False Negatives (FN). Predictions were evaluated at confidence levels ranging from 0.00 to 1 in increments of 0.05. The optimal confidence levels for each method were selected based on the highest F1-score, the harmonic mean of precision and recall (Table 3). For the PlasticModel, the confidence thresholds determined for free-floating plastics were used.

Table 3: Highest F1 values found per model and method and the corresponding confidence thresholds. For GoPro entangled plastics, the applied threshold of 0.10 corresponded to an F1 of 0.47.

Model	Class	Method	$F1_{max}$	Confidence threshold	Confidence threshold applied
HyacinthModel	Hyacinths	UAV	0.72	0.30	0.30
		GoPro	0.61	0.20	0.20
PlasticModel	Free-floating plastics	UAV	0.36	0.45	0.45
		GoPro	0.30	0.10	0.10
	Entangled plastics	UAV	0.45	0.45	0.45
		GoPro	0.61	0.30	0.10

Post-processing of object detection output

All FOVs and bounding boxes were recalculated from pixels to surface area in square meters [m²]. Recalculations were performed using the Ground Sampling Distance (GSD) [cm/pixels]:

$$GSD = \frac{S_w \times H}{F_l \times \omega_i}$$

, where H is the camera height, S_w is the camera sensor width, F_l the camera focal length $[\mathrm{mm}]$, and ω_i the image width in pixels[51]. Except for height, all variables in this equation remained constant per UAV or GoPro. Height for UAV was retrieved using ExifTool[52] and specified per image. For GoPro imagery, the in-field reported height per waypoint per bridge, averaged over tides, was used.

All WH bounding boxes were corrected by factor 0.79 to comply with the predominant ellipse shape of WH patches[23]. All instances where entangled plastics but no WHs were identified were manually cross-checked (n = 164). Cases where the image was fully covered by WHs were corrected with the same area as the FOV (n = 138). Others with partial WH coverage were corrected by FOV multiplied with the ellipse factor (n = 11). For all other cases hyacinth area was kept 0 (n = 15). In cases where the WH coverage exceeded the FOV, (n = 202), the corrected area was calculated as FOV × 0.79, assuming that the overlaying bounding boxes resulted from multiple single WH patches.

Additionally, uncorrected bounding boxes of detected plastics (both free-floating and entangled) were grouped into 11 size classes from 0.01–0.1 up to 0.9–1.0 and above 1.0 m². For both

UAV and GoPro images, up to 10 images per class were used as input, and object detection was applied based on a 0.1 confidence level. All retrieved bounding boxes were examined, and the ground truth object type was noted. The majority of objects in size classes above 0.1 m² were not plastics, and the majority of detected objects also fall within this class size (Figure S2). Plastic size or size filtering was not further applied or used for plastic–WH interaction metrics.

Plastic–water hyacinth interaction metrics

With the retrieved bounding boxes of WHs, counts of free-floating and entangled plastics, and FOVs, the following metrics are calculated: trapping ratio [-], water hyacinth surface coverage [m²], water hyacinth patch size [m²], the total river surface plastic concentration C_r [#/km²], the non-hyacinth-covered (open) surface plastic concentration C_o [#/km²], the concentration plastics inside hyacinths C_{wh} [#/km²], and consequently the ratios C_{wh}/C_r and C_{wh}/C_o, which compare plastic concentration in hyacinths to the total river and open water concentrations, respectively. Calculations are shown in Table S5.

Statistical analysis

Normality of the data was assessed using the Shapiro–Wilk test. As normality was not found, differences between distance categories were evaluated using the non-parametric Kruskal–Wallis test. Relationships between relevant metrics and distance to the Gulf of Thailand were assessed using Spearman's rank correlation, which is robust to non-normal distributions and captures correlation without assuming linearity. The correlation is based on the mean values per location. Statistical significance was defined at $p < 0.05$. The minimum and maximum values per location, over the complete field work period, are also calculated and included as error bars.

RESULTS

Object detection is transferable for hyacinths and entangled plastics

The YOLOv8 HyacinthModel trained on Saigon River shows only a small 2% mAP50 drop when deployed on Chao Phraya, decreasing from 70% to 68%. The PlasticModel accuracy differs per class. While entangled plastics detection has 54% mAP50 (vs. 52% in Saigon), free-floating plastics detection performs notably worse in Chao Phraya at 23% mAP50 compared to 48% in Saigon. While the classes hyacinths and entangled plastics transfer relatively well, the transferability of detecting free-floating plastics is limited (Table 4). The poor performance could be attributed to site-specific characteristics of the water surface, such as sediment levels, water color, flow velocity, wave patterns, sunglint and the dominant plastic items per region. The composition of plastics, and consequently the distribution of plastic sizes, differs greatly per river and within rivers[28,30], possibly underestimating certain plastic types that are prevalent in different regions. These variable circumstances suggest that free-floating plastic detection could benefit from a highly diverse and complete training set for global transferability, or river-specific calibration for a targeted river. Figure S4 further shows the distribution of detected size classes and occurrence and relationship with sunglint, also highlighting the importance for future work on detection performance and site-specific characteristics.

The good performance of the HyacinthModel can be attributed to the consistent size and color characteristics of WHs that make their detection well transferable across river systems. Similar, these characteristics of WHs serve as a distinctive background for entangled plastics[23], which may enhance the transferability of their detection, especially compared to free-floating

litter against the variable water surface background. Under sunglint conditions, the distinction between sunglint on the water surface and white or transparent free-floating litter items becomes less clear. As a result, the model often fails to detect such free-floating litter[53], as shown in Figure 4. Additionally, both models used the same training set, with all three classes. Training three separate models, one for WHs, one for free-floating plastics, and one for entangled plastics may improve overall performance of detection of each class. This approach could also enhance the transferability across river systems, as the results suggest that only the free-floating plastic model would benefit greatly from retraining. However, using multiple separate models will make the monitoring process more complex.

Table 4: Model performance evaluation shows only a small accuracy when evaluating the Saigon-trained YOLO model on the Chao Phraya River. A default confidence threshold of 0.5 is used for this model performance evaluation

Model	Class	Chao Phraya River (this study)				Saigon River (comparison[24])			
		Precision	Recall	(m)AP50	(m)AP50–95	Precision	Recall	(m)AP50	(m)AP50–95
HyacinthModel	Water Hyacinth	0.80	0.544	68%	49%	0.83	0.54	70%	48%
PlasticModel	Free-floating plastics	0.290	0.192	23%	16%	0.72	0.25	48%	37%
	Entangled plastics	0.522	0.312	54%	35%	0.69	0.39	52%	38%

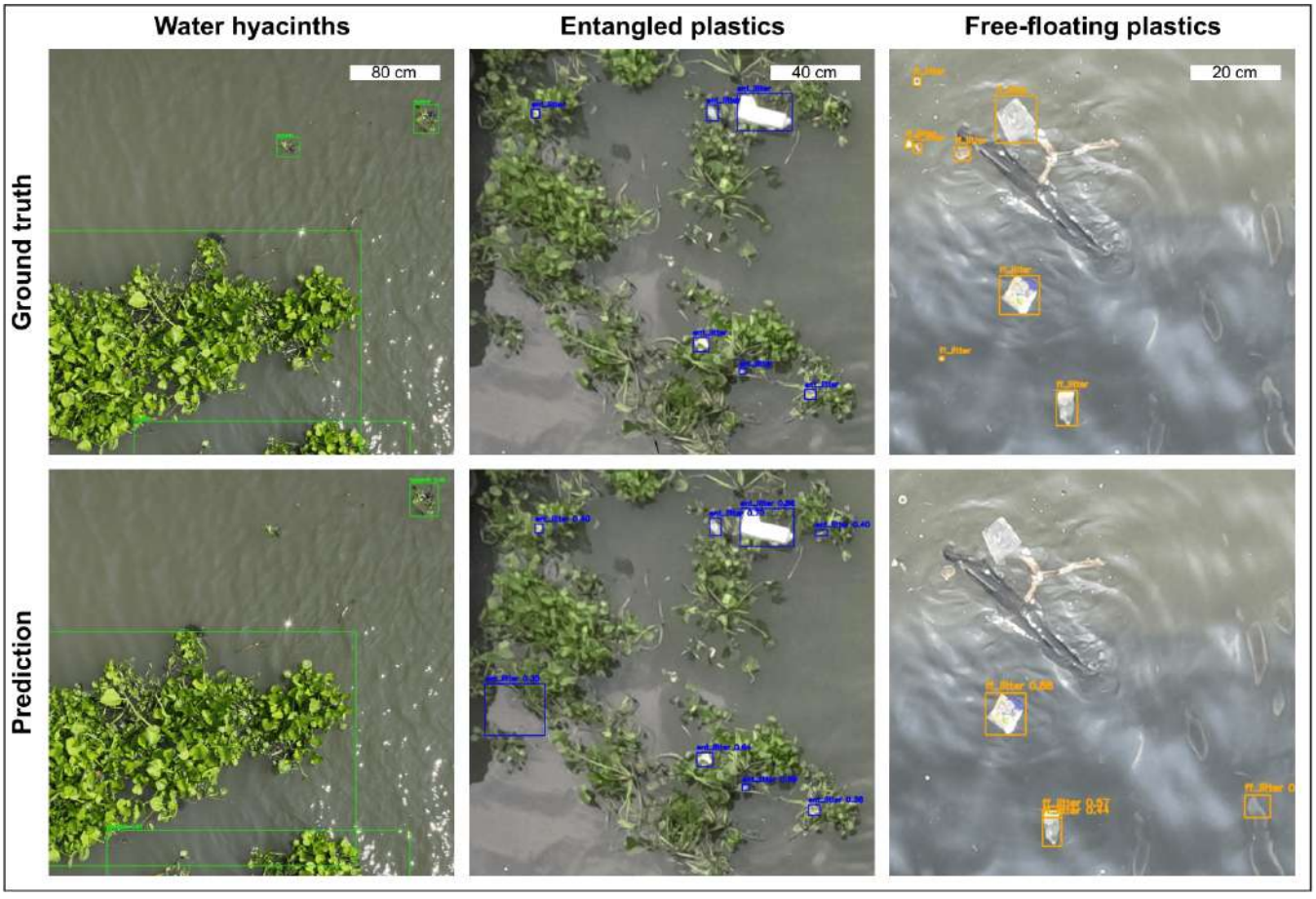

Figure 4: Examples of hand-annotated ground-truth bounding boxes (top) compared to predicted bounding boxes (bottom) for (left) water hyacinths, (middle) entangled plastics, and (right) free-floating plastics. Scalebars differ between panels due to varying spatial resolution.

Water hyacinth coverage decreases in downstream direction

Water hyacinth pixel classification from Sentinel-2

The application of the Sentinel-2 WH detection algorithm classifies pixels at a spatial resolution of 10 × 10 m. Figure 5 shows the classification for a partial Sentinel-2 scene acquired on 16 March 2025. Figure S1 shows the spectral signatures and the difference between WHs and open water from hand-annotated 10 × 10 m Sentinel-2 pixels (n = 600) from the Saigon River, as reported by Janssens et al.[25].

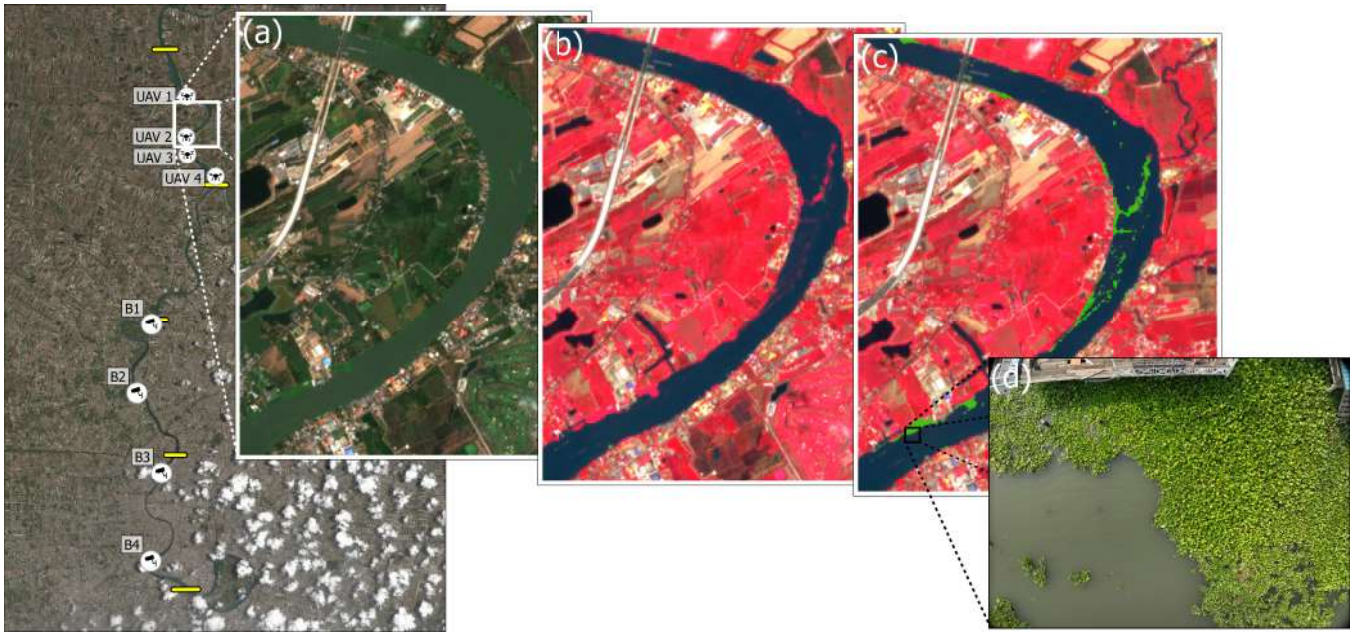

Figure 5: (a) True-color Sentinel-2 imagery acquired on 16 March 2025. (b) The same image displayed in false-color composite of the water column prior to classification. (c) The same image but with water hyacinth pixels classified and highlighted in green. (d) UAV image taken at location UAV 2 on March 20. This example of a WH patch retained between building structures is used as no Sentinel-2 imagery with suitable cloud conditions was available on the same date as in-situ imagery at any location. The reference map on the left indicates the location within the study area.

Spatial variation

The mean classified WH area differed significantly among distance categories between June 2024 and 2025, as indicated by a Kruskal–Wallis test (χ^2 = 20.98, df = 3, p = 0.0001). The annual average WH coverage, shown in Figure 6a, was 2.05%, ranging between 2.34% lower midstream and 1.55% downstream. A decreasing trend of WH coverage towards the river mouth is supported by a positive Spearman correlation, however the significance of the correlation is weak (ρ = 0.16, p = 0.1035, n = 108). Throughout the study period, Sentinel-2 detects an average WH coverage of 1.81% across the study period, decreasing from average 2.44% upstream to 0.92% downstream, shown in Figure 6b. This declining spatial trend (Spearman, ρ = 0.46, p = 0.0425, n = 20) is consistent with findings from the Saigon River[25]. Object detection during the same period showed a similar trend, although not significant (ρ = 0.62, p = 0.1017, n = 8). Compared to Sentinel-2, object detection revealed a higher WH coverage upstream by a factor of 1.3 (UAV1) to 7 (UAV3), and lower coverage downstream by a factor of 0.1 (B1) to 0.4 (B3).

WH coverage and mean patch sizes [m²] are lower downstream (Figure 7), likely due to

disruption of mats by increased boat traffic and riverine infrastructure ,[22]. This pattern further reflects the higher and cumulative urbanization along the lower Chao Phraya, both within and outside the Bangkok Metropolitan Region, compared to upstream areas[54]. Additionally, stronger flow velocities or greater tidal forces may lead to fragmentation[55]. These fragmented, but often dense clusters of small patches downstream may still fully occupy 10 × 10 meter pixels in Sentinel-2 imagery, possibly explaining the higher values observed in Sentinel-2 data compared to bridge-based estimates[25]. However, to validate this, the density of smaller patches [#/m^2] should be investigated, as well as the minimum hyacinth coverage required for Sentinel-2 to classify a pixel as water hyacinth. UAV and bridge imagery can here validate and mitigate the resolution issues of Sentinel-2. On the other hand, the differences between Sentinel-2 and object detection are likely influenced by differences in spatial coverage and the degree of extrapolation required. Bridge and UAV imagery capture only a limited portion of the river, missing the broader variability visible in Sentinel-2 scenes, which can lead to mismatches in estimated coverage.

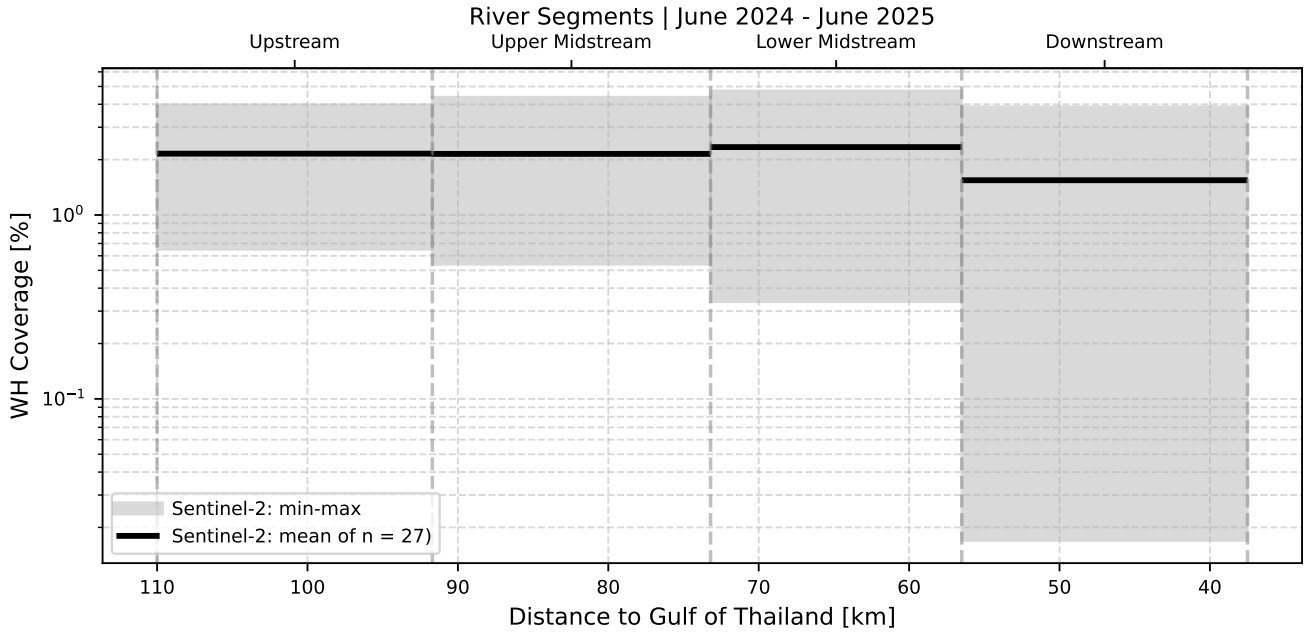

(a)

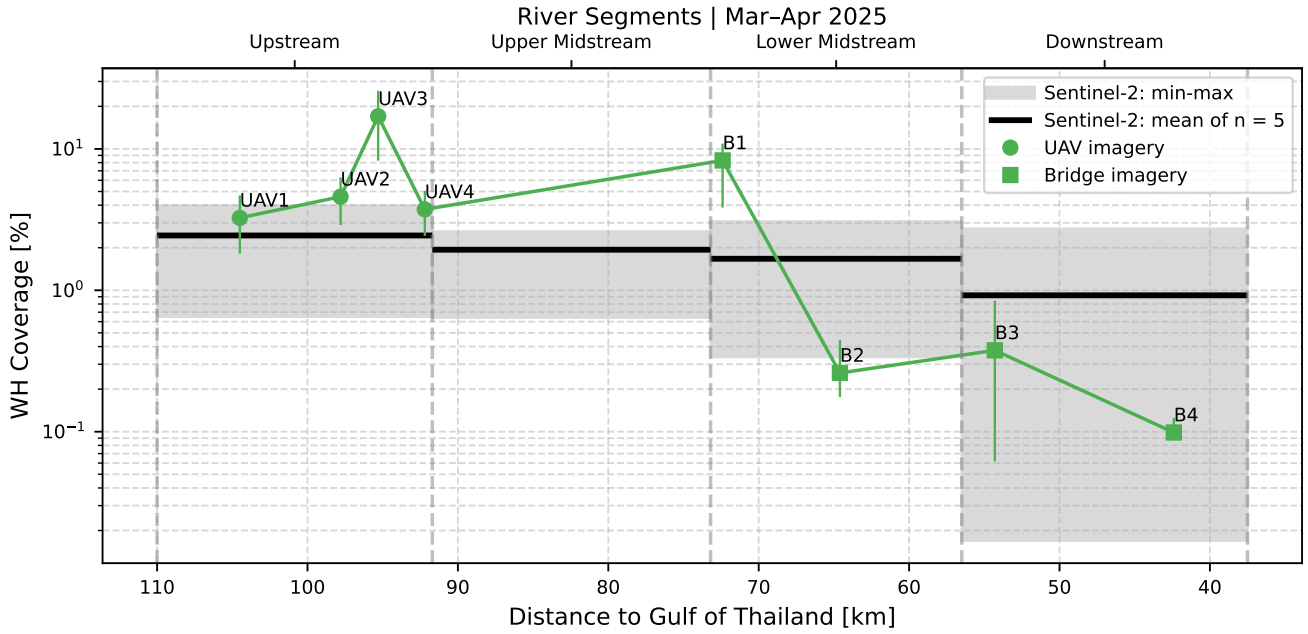

(b)

Figure 6: WH coverage along river segments: (a) June 2024–June 2025 retrieved with Sentinel-2 (b) March–April 2025 with UAV and bridge imagery, compared to Sentinel-2 results. Data are represented as mean with minimum and maximum as error bars.

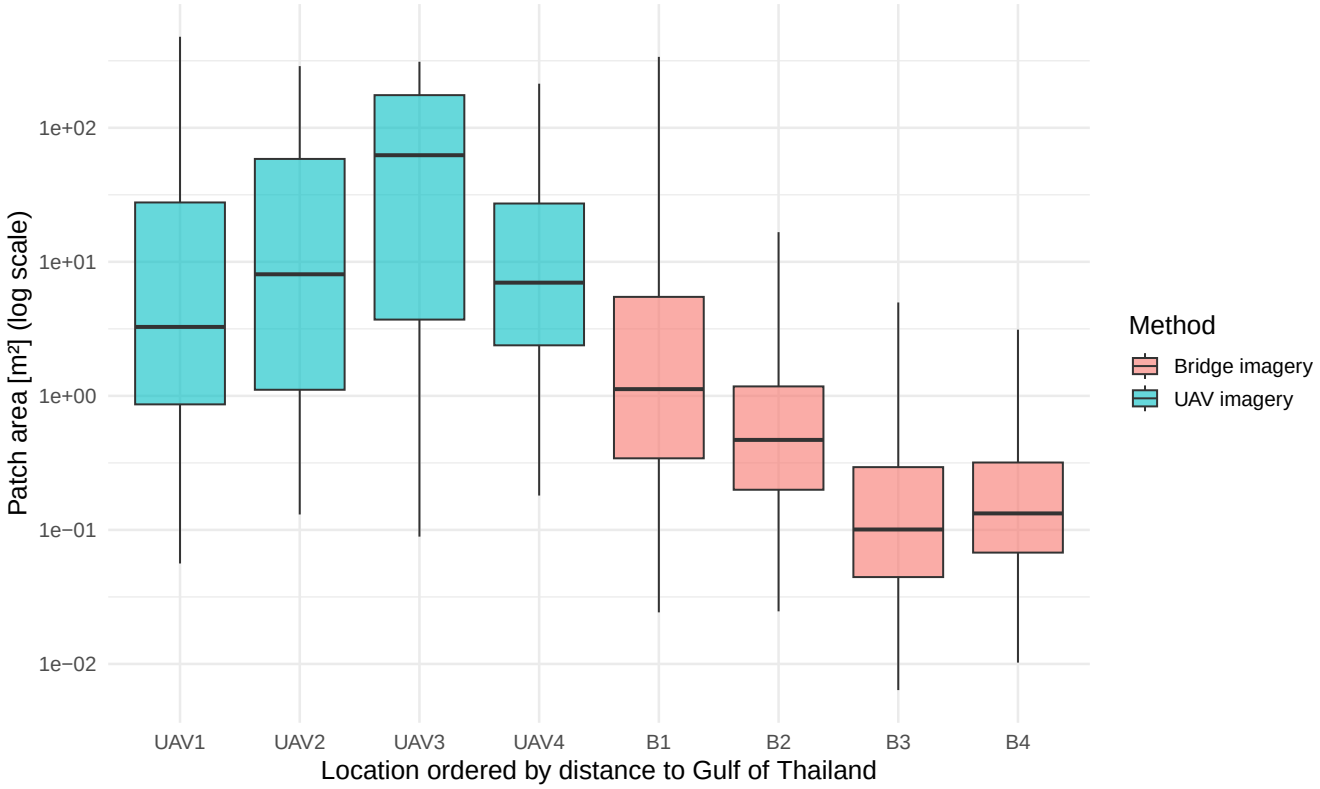

Figure 7: Mean patch sizes are up to a factor 162 larger upstream (UAV3) than downstream (B3). Maximum patch size is limited by the camera FOV. Data are represented as boxplots with the minimum and maximum as error bars.

Seasonal variation

Figure 8 shows an higher WH coverage (%) in the dry season, between November and February. This is similar to seasonal patterns observed in the Saigon River[25]. Both regions show seasonality in the dry season, with low cloud cover. However, cloud cover poses a great uncertainty in the actual seasonality trend. In the Chao Phraya, only five images are available between July to December 2024. Additionally, WH coverage is not consistently highest during the dry season across all regions[26]. Moreover, WH coverage over the spatial extent can be influenced by river obstructions, introducing variations that are independent of seasonal patterns, as is the case for the Chao Phraya[56]. Therefore, the use of Sentinel-1 SAR data should be considered to map the spatial and temporal variation of WHs[12].

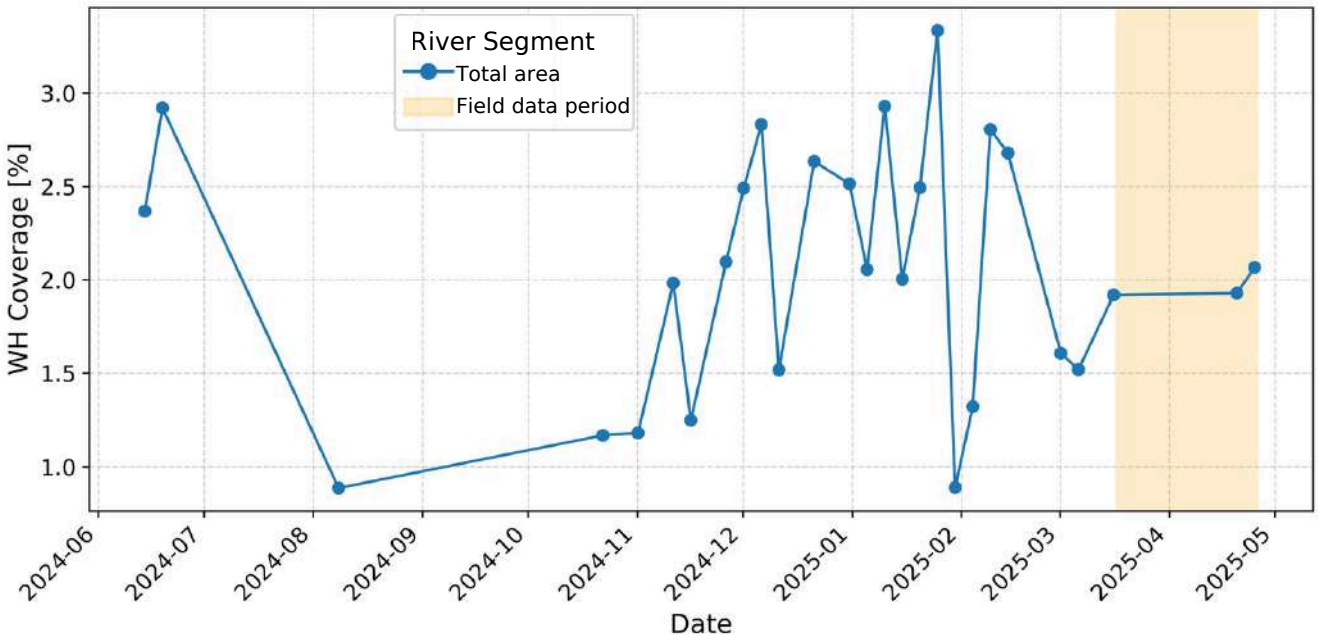

Figure 8: During the dry season, WH coverage was higher than during the hot and rainy seasons. Between June and December 2024, only five images were available compared to 22 between December 2024 and June 2025.

Plastic concentration in hyacinths increases in downstream direction

Figure 9a shows that the trapping of plastics inside WHs decreases towards the Gulf of Thailand (Spearman, ρ = 0.93, p = 0.0022, n = 8). Averaged over all locations and periods, 32% of all plastics were found within WHs, ranging from 78% (UAV3) to 1.3% (B4). Only at the three most upstream locations, hyacinths carried the majority of floating plastics, with trapping ratios of 66% (UAV1), 53% (UAV2), and the highest location-specific mean of 78% at UAV3. It is still unclear what explains the lower trapping ratios downstream segments. The plastic flux still increases in the downstream direction, suggesting that there may be simply more plastics than the WHs can carry (plastic saturation), dependent on the season and influenced by higher and cumulative urbanization along the river downstream[54], with higher amount of plastics and the disruption of WH patches. Visual counting and bridge imagery show similar trapping ratios across B1–B4, with small point-wise differences (-0.08 – 0.05). This consistency reinforces the validity of the results and improves transferability of using one or both of these methods. A reducing trapping ratio towards the ocean was also found in the Saigon, although with a much higher average trapping ratio of 73%[23]. This emphasizes the variability of the capacity of WHs in plastic transport along both the spatial extent and among river systems.

In contrast to a negative trend in trapping ratio towards the sea, there is a increasing trend downstream of total number of entangled items per km² water hyacinths C_{wh} [#/km²] (Spearman, ρ = -0.81, p = 0.0218, n = 8) (Figure 9b). C_{wh} averages at $1.4{\cdot}10^6$, and ranges from $3.1{\cdot}10^4$ (UAV2) to $8.8{\cdot}10^6$ (B3). Correspondingly, total river surface plastic concentration C_r and open water surface plastic concentration C_o [#/km²] both increase downstream, with Spearman correlations of ρ = –0.91 (p = 0.0046) and ρ = –0.95 (p = 0.0011), respectively. Plastic fluxes show a similar pattern, increasing from 1,114 (B1) to 20,025 (B4) items per hour, which is both smaller and larger than previously reported by van Calcar & van Emmerik[30], who observed fluxes between 2,460 and 5,340 items per hour 20 to 30 km from the river mouth.

The relative contribution of plastic concentration in water hyacinths (C_{wh}) compared to open

water (C_o) varies significantly, ranging from 20 times higher at location UAV4 to 142 times higher at location B3 (Figure 9c). The highest ratios are observed at the upstream and downstream locations, with plastic concentrations in hyacinths being 80 times higher than in open water at UAV1, 142 times higher at B3 and 107 times higher at B4. This indicates that WHs in these areas act as strong plastic accumulation zones.

Previously, the increase in C_{wh} downstream was associated with reduced hyacinth coverage and a slight drop in trapping ratio, C_r and C_o for the Saigon River[24]. This does not hold for the Chao Phraya, where trapping ratios drop sharply from 73% to 1.3% and C_r and C_o both increase. At the same time WH coverage is low, and C_{wh}/C_o is high downstream. This suggests that the sparse hyacinths accumulate high densities of plastic, arguably due to higher exposure to the overall plastic concentration in the river (C_r) downstream, however further research on the trapping mechanisms is needed. Therefore, it could be assumed that the trapping ratio is the driver of high C_{wh}/C_o values upstream, while downstream WHs and plastics may mainly co-occur due to a similar response to the river flow dynamics, resulting in joint concentration.

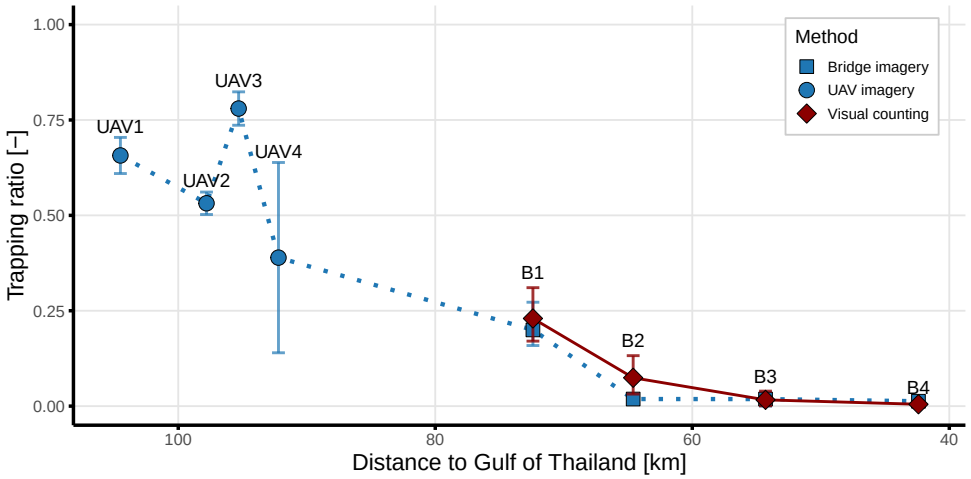

(a)

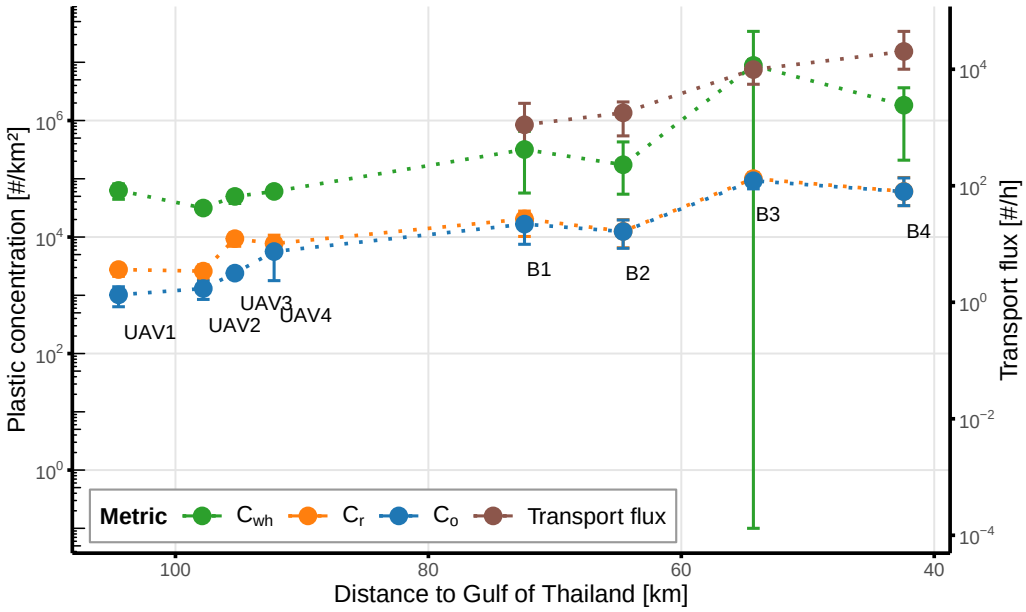

(b)

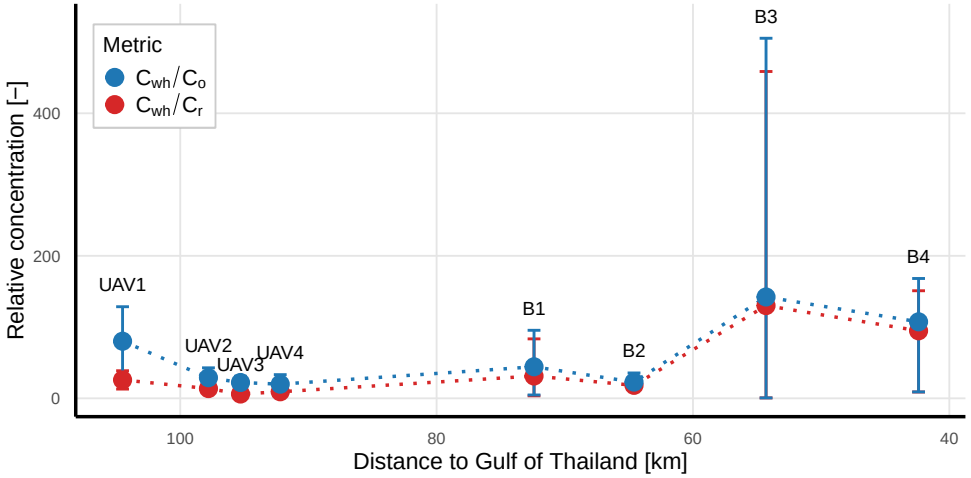

(c)

Figure 9: a) Trapping ratio, b) Plastic concentration in water hyacinths (C_{wh}), in open water (C_o), and of the total river surface (C_r) are shown on the first y-axis, with plastic flux on the second y-axis. The global average of C_{wh} is 59 times higher than that of C_o, c) Relative concentrations of plastics: C_{wh}/C_o and C_{wh}/C_r. Data are represented as mean with minimum and maximum as error bars.

Physical sampling shows underestimation of entangled plastics

Plastic concentration by physical sampling

Physical sampling found approximately 74 plastic items per m^2, compared to 5.3 items per m^2 from bridge imagery within the same area as physical sampling (Table 5). The estimated hyacinth area (m^2) and retrieved hyacinth mass (kg) suggest a wet biomass of approximately 8 kg/m^2 in the study area, comparable to the 10 kg/m^2 reported by[57] for low-density conditions. Sampling occurred in downstream locations with sparse, fragmented patches, consistent with such low-density hyacinth distributions. The higher concentration of plastics shown in physical sampling is in line with those in the Saigon river[22]. This supports the idea that hyacinth's traits, such as the extensive root structures, contribute to plastic trapping mechanisms. Additionally, bridge imagery likely missed plastics, as it usually fails to detect submerged items and transparent litter. In addition, the detection of small plastics often fails[53]. Moreover, physical sampling included submerged, transparent and small plastics ($\geq$ 0.5 cm), the difference in items per m^2 between bridge imagery and physical sampling can be explained.

Table 5: Plastic concentration entangled in water hyacinths.

Measuring technique	Plastic items per m^2	Mass concentration (g/kg)
Physical sampling	73.91	25.06
Bridge imagery (B3 + B4)	5.33	N/A

Distribution of plastic types

Figure 10 shows the composition of plastic types, as retrieved from physical sampling and visual counting. Visual counting indicates a higher proportion of EPS and PET inside WHs compared to outside, with 23% vs. 4% for EPS and 10% vs. 1% for PET, respectively. This is similar to ratios found in Schreyers et al.[27]. PO soft and PO hard display similar and predominant proportions both inside and outside hyacinths. Rubbers are found in a considerably higher portion outside hyacinths during visual counting (6% compared to 24%). However, physical sampling shows rubbers accounted for 25%. This could be attributed to the entanglement-prone structure of rubbers, easily getting trapped in hyacinth roots (Figure S6). Physical sampling shows a higher proportion of PO hard, and a lower proportion of PO soft and PET compared to visual counting. These differences could be influenced by the location where physical sampling was performed, given the plastic type concentrations found with visual counting (Figure S7).

The mass distribution further shows a higher proportion of PET, likely due to its large size class and generally unfragmented state[22]. Although the count of rubbers is high, their mass contribution remains low, as the category mainly consists of small, lightweight, elastic bands. Other plastics mostly consisted of lighters (full or empty), contributing more to mass. The mean mass per plastic type can be found in Table S8.

Our plastic type categorization in the Chao Phraya may assist local and national policymakers in identifying the most problematic plastic types for targeted mitigation measures. However, this categorization could be further improved through laboratory-based identification and exploratory studies on the dominant plastic types used for plastic items in different regions.

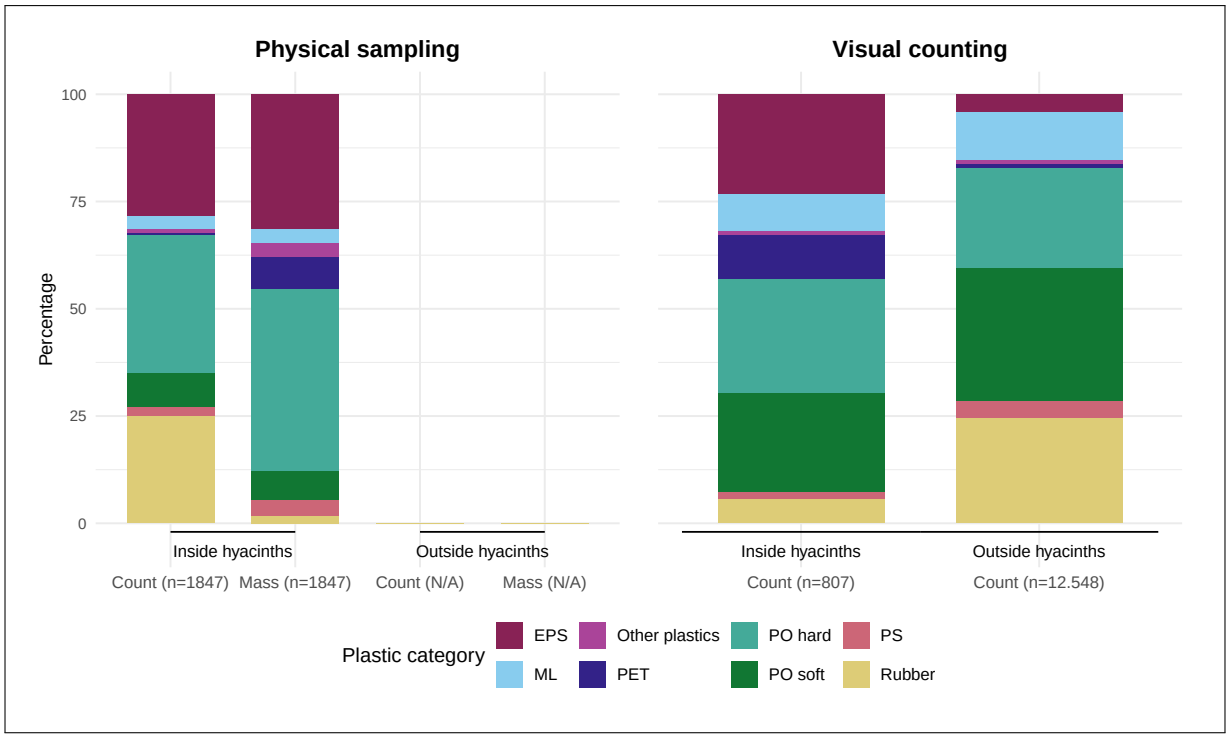

Figure 10: Physical sampling yielded both count and mass information of 8 distinct plastic categories. This figure shows how it relates to the categorized count data retrieved with visual counting. Physical sampling solely focuses on plastics inside water hyacinths, whereas visual categorization includes counting data both in and outside water hyacinths.

Discussion

Transferability of plastic-water hyacinth interactions

One of the main objectives of this research was to test the transferability of plastic-water hyacinth interactions, and field-based and remote sensing detection methods. Most scientific work on plastic-water hyacinth interactions have been done on the Saigon River, Vietnam. Numerous anecdotal reports are available on similar processes in other rivers, including the Rio Ozama (Dominican Republic[58]) and the Citarum (Indonesia[59]).Yet, our paper is the first study to quantitatively describe and analyze the trapping of plastic pollution by water hyacinths in another river system, the Chao Phraya. The available methods for water hyacinths detection from space[25], and protocols to quantify the river-scale trapping of plastic using cameras, drones, and field sampling[22], were directly applicable to this river system. We are therefore confident that our combined work on these rivers can be further transferred to other rivers around the world, although adaptations may be required due to local circumstances and limitations.

Limitations of the study

While this paper provides valuable research about the transferability of plastic-hyacinth relationships and detection models, several limitations require acknowledgment. First of all, the elaborate data collection over a 62.1 km extent yielded images with broad variance in camera height. These differences in camera height influenced the image resolution and potentially the minimum detectable plastic item size. However, cross-validation with previous research and simultaneous data-collection methods support the time and space-averaged results in this study. Further re-

search into the spatial distribution of the plastic sizes of both entangled and free-floating plastics could help quantify these limitations. Second, post-processing included cross-evaluation of true hyacinth coverage, but was only performed on images where hyacinths were not detected, yet entangled plastics were. As a result, the results may underrepresent total hyacinth coverage and could be biased toward scenes where entanglement occurred. This potential bias could be accounted for in the future by applying systematic post-processing after object detection or by using segmentation for more accurate hyacinth detection, as demonstrated on UAV images by Schreyers et al.[22]. Third, tests of model transferability were limited to comparisons of model evaluation output, for object detection, and evaluation based on direct results for Sentinel-2. It is suggested that future research dives deeper into the generalization capacity of the models by, for example, testing the performance again after adding a small proportion of Chao Phraya training data to the training set, similar to what was done by van Lieshout et al.[60]. This would help assess how much additional data from another river system can improve model performance and transferability.

Outlook to future work

Based on the global overlap of highly polluted rivers and thriving habitats for water hyacinths, we expect that plastic-water hyacinth interactions are relevant in many other systems around the world. We therefore suggest to further test the transferability of these interactions and detection methods in other rivers with different geomorphological, hydrological, and plastic pollution characteristics. Additionally, evaluating sampling methods across varying drivers and environmental conditions, such as plastic loads, human presence, and river complexity, would support their harmonization and improve their reliability across different sites[61,62]. Although the Chao Phraya and Saigon rivers differ on many aspects, they are also similar in terms of width, discharge, tidal dynamics, climate and connection to densely populated areas. Smaller rivers and urban channels may reach much higher water hyacinth coverage proportions, and it is still unresolved how this may affect the trapping of plastic pollution. Furthermore, the remote sensing based water hyacinth detection methods may work less accurate due to the limited spatial resolution of Sentinel-2. Additional satellite imagery with higher resolution may offer additional opportunities for monitoring water hyacinths in such systems[12,63]. The applicability to large rivers should also be investigated further, such as the Amazon, Mekong, or Nile. These river basins are known to contribute to global plastic pollution and to faces challenges from water hyacinth growth[64–66]. The exact processes that result in trapping of plastics in water hyacinths remain unresolved. From anecdotal evidence, it has become clear that the high correlation between plastic pollution and water hyacinths can be both attributed to trapping of plastics on and within the plants, and the co-occurrence of plastics and plant material[24]. More detailed experiments, including tracking experiments, time lapses, or lab experiments may shed additional light on what factors determine the trapping and co-occurrence of plastics and water hyacinths in river systems. Similarly, the release mechanisms remain unknown, and it is unclear of this is driven by disintegration of the plant, or escaping of the plastic items from the plant. The plastic characteristics may also play an important role here. In both the Chao Phraya and Saigon, large portions of expanded polystyrene (EPS; foam) were found within the water hyacinths. However, it is clear that the composition of plastic pollution varies considerably between rivers around the world. For example, in European rivers higher portions of soft plastics are found, which are also often found in riparian vegetation[30,67]. The effect of plastic characteristics on the trapping rate in water hyacinths remains unresolved. Future work may also extend to smaller plastics, including microplastics and nanoplastics (MNP). Previous work has found that water hyacinths can effectively take up MNPs[68,69], it remains however unclear if water hyacinths concentrate MNPs as much as floating macroplastics.

Conclusion

Water hyacinths function as macroplastic aggregators in multiple river systems around the world and this is therefore a transferable phenomenon. This research finds that water hyacinths trap up to 78% of all floating riverine macroplastics, and 32% on average over a 62.1 km spatial extent along the Chao Phraya River, Thailand. It was found that the trapping ratio and WH coverage show a decreasing pattern towards the river mouth. At the same time, we found that the concentration of plastics inside hyacinths increases in this direction. This paper suggests that the high plastic concentrations upstream are related to the plastic trapping capability of hyacinths. At locations where hyacinths are less abundant, downstream in this case, this research suggests that plastics and hyacinths jointly concentrate and co-occur due to a similar response to river flow dynamics.

Sentinel-2 shows both its strengths and weaknesses. The overall detection capability of the Naive-Bayes classifier is promising, showing trends comparable to earlier research and cross-validation within this study. The free availability and high resolution of the data is promising for scalability, however, cloud-cover poses a serious limitation for mapping temporal and spatial fluctuations, given the water hyacinths variability in seasonality and distribution.

Object detection functions as a transferable approach to investigate plastic-hyacinth interactions, although limited for the detection of free-floating plastics. Free-floating debris and regional river characteristics may be too variable for the model. Training specialized models specifically for free-floating plastics may improve transferability to other river systems.

This paper is the first to evaluate the plastic-trapping role of water hyacinths from large and small scale using satellite remote sensing, drones, camera imagery, object detection and extensive in-field measurements. Additionally, it expands investigation of plastic-hyacinth interactions to a new geographical context, the Chao Phraya, and covers the longest spatial extent examined in this context to date. Ultimately, this study supports the use of water hyacinths as a transferable proxy in hyacinth-infested and plastic-polluted rivers worldwide. The use of this proxy could eventually support the development of large-scale plastic pollution monitoring strategies and targeted clean-up efforts.

RESOURCE AVAILABILITY

Lead contact

Requests for further information and resources should be directed to and will be fulfilled by one of the lead correspondents, Giel W.A. Hagenbeek (giel.hagenbeek@wur.nl) and Tim H.M. van Emmerik (tim.vanemmerik@wur.nl).

Materials availability

This study did not generate new materials.

Data and code availability

- The Sentinel-2 image data used in this work are part of the Copernicus Sentinel programme and are freely available through the Copernicus Data Space Ecosystem. The access and processing of the data was performed through Sentinel Hub (Enterprise account), which was sponsored by the ESA Network of Resources (NoR). All UAV and GoPro imagery is publicly available at `https://doi.org/10.4121/f771da08-8143-4a4b-9ad6-c8e711812a63.v1`, just like the object detection results, annotations, physical sampling and visual counting data.
- All original code has been deposited at 4TU and is publicly available at `https://doi.org/10.4121/f771da08-8143-4a4b-9ad6-c8e711812a63.v1`. The water hyacinths classification tool using Sentinel-2 is available at `https://github.com/GielHagenbeek/Waterhyacinth_classification_Sentinel2`. The original YOLOv8 code is available at `https://github.com/TianlongJia/deep_plastic_YoloV8`[70]

ACKNOWLEDGMENTS

We are very thankful to Mr. Thanaphol Boodchuang (Asian Institute of Technology) who assisted with the fieldwork as drone pilot. We also acknowledge Ms. Chollada Phumsaard together with the municipal staff of the Bangkok Metropolitan Administration (Yellow Boat) for their contributions to the physical sampling campaign. Further thanks go to Mr. Kathawut Prasarnnin and Ms. Nadhira Sagita Putri (The Ocean Cleanup) for the introduction and coordination with the Interceptor 019 team in Bangkok. Special thanks go to Parattakorn Areerungruang and Makkatin Praphan from Miles Up Run Club for the warm welcome in Bangkok. Additionally, we thank everyone who helped and showed support throughout the process, especially Bianka Fábryová, Conor Murphy, Niek Westerink, Judith Hagenbeek, and Willem Hagenbeek. This work was supported by the ESA Network of Resources (NoR) sponsorship (5210ul).

AUTHOR CONTRIBUTIONS

Conceptualization: G.W.A.H, T.v.E., M.R.; Data curation: G.W.A.H; Formal analysis: G.W.A.H; Funding acquisition: G.W.A.H, M.R.; Investigation: G.W.A.H; Methodology: G.W.A.H, T.J., R.T.; Project administration: G.W.A.H, K.B., P.K., T.v.E., M.R.; Resources: G.W.A.H, K.B., P.K., T.J.; Software: G.W.A.H., M.R., T.J.; Supervision: T.v.E., M.R.; Validation: G.W.A.H; Visualization: G.W.A.H.; Writing - original draft: G.W.A.H, T.v.E.; Writing - review & editing: all authors.

DECLARATION OF INTERESTS

The authors declare no competing interests. Thomas Mani is employed by The Ocean Cleanup, a non-profit organization aimed at advancing scientific understanding and developing solutions to rid the oceans of plastic.

STAR METHODS

Detailed methods are provided in the online version of this paper and include the following:

- **Key Resource Table**
- **Method Details**
  - Overall Methodology
  - Study Area
  - Bridge-mounted camera imagery
  - UAV Imagery
  - Visual Counting
  - Physical Sampling
  - Sentinel-2 Data and Application
  - Object Detection Data and Application
  - Model Performance Evaluation
  - Model Output Settings
- **Quantification and statistical analysis**

SUPPLEMENTAL INFORMATION INDEX

Document S1. Figures S1,S4, S6, S7 and Tables S2,S3,S5, S8

References

1. van Emmerik, T., and Schwarz, A. (2020). Plastic debris in rivers. Wiley Interdisciplinary Reviews: Water *7*, e1398.

2. Meijer, L.J.J., van Emmerik, T., van der Ent, R., Schmidt, C., and Lebreton, L. (2021). More than 1000 rivers account for 80% of global riverine plastic emissions to the ocean. Sci. Adv. *7*. doi: 10.1126/sciadv.aaz5803.

3. Lau, W.W., Shiran, Y., Bailey, R.M., Cook, E., Stuchtey, M.R., Koskella, J., Velis, C.A., Godfrey, L., Boucher, J., Murphy, M.B. et al. (2020). Evaluating scenarios toward zero plastic pollution. Science *369*, 1455–1461.

4. van Emmerik, T.H., Kirschke, S., Schreyers, L.J., Nath, S., Schmidt, C., and Wendt-Potthoff, K. (2023). Estimating plastic pollution in rivers through harmonized monitoring strategies. Marine Pollution Bulletin *196*, 115503.

5. Maximenko, N., Corradi, P., Law, K.L., Van Sebille, E., Garaba, S.P., Lampitt, R.S., Galgani, F., Martinez-Vicente, V., Goddijn-Murphy, L., Veiga, J.M., Thompson, R.C., Maes, C., Moller, D., Löscher, C.R., Addamo, A.M., Lamson, M.R., Centurioni, L.R., Posth, N.R., Lumpkin, R., Vinci, M., Martins, A.M., Pieper, C.D., Isobe, A., Hanke, G., Edwards, M., Chubarenko, I.P., Rodriguez, E., Aliani, S., Arias, M., Asner, G.P., Brosich, A., Carlton, J.T., Chao, Y., Cook, A.M., Cundy, A.B., Galloway, T.S., Giorgetti, A., Goni, G.J., Guichoux, Y., Haram, L.E., Hardesty, B.D., Holdsworth, N., Lebreton, L., Leslie, H.A., Macadam-Somer, I., Mace, T., Manuel, M., Marsh, R., Martinez, E., Mayor, D.J., Le Moigne, M., Molina Jack, M.E., Mowlem, M.C., Obbard, R.W., Pabortsava, K., Robberson, B., Rotaru, A.E., Ruiz, G.M., Spedicato, M.T., Thiel, M., Turra, A., and Wilcox, C. (2019). Toward the integrated marine debris observing system. Frontiers in Marine Science *Volume 6 - 2019*. URL: https://www.frontiersin.org/journals/marine-science/articles/10.3389/fmars.2019.00447. doi: 10.3389/fmars.2019.00447.

6. UNEP. Zero-draft text of the international legally binding instrument on plastic pollution, including in the marine environment. Tech. Rep. United Nations (2023).

7. Tasseron, P., van Emmerik, T., Peller, J., Schreyers, L., and Biermann, L. (2021). Advancing floating macroplastic detection from space using experimental hyperspectral imagery. Remote Sensing *13*. doi: 10.3390/rs13122335.

8. Themistocleous, K., Papoutsa, C., Michaelides, S., and Hadjimitsis, D. (2020). Investigating detection of floating plastic litter from space using sentinel-2 imagery. Remote Sensing *12*. doi: 10.3390/RS12162648.

9. Topouzelis, K., Papageorgiou, D., Suaria, G., and Aliani, S. (2021). Floating marine litter detection algorithms and techniques using optical remote sensing data: A review. Marine Pollution Bulletin *170*. doi: 10.1016/j.marpolbul.2021.112675.

10. Blume, S., Franke, J., Garaba, S., Giang, P., Mathis, J., Ortwig, N., and Ziegler, S. Advances in remote sensing of plastic waste. Tech. Rep. Deutsche Gesellschaft für Internationale Zusammenarbeit (GIZ) GmbH Bonn and Eschborn, Germany (2023). URL: https://www.giz.de/en/downloads/giz-2023-en-advances-in-remote-sensing-of-plastic-waste.pdf gIZ Report; Accessed: 2025-01-10.

11. Martínez-Vicente, V., Clark, J.R., Corradi, P., Aliani, S., Arias, M., Bochow, M., Bonnery, G., Cole, M., Cózar, A., Donnelly, R., Echevarría, F., Galgani, F., Garaba, S.P., Goddijn-Murphy, L., Lebreton, L., Leslie, H.A., Lindeque, P.K., Maximenko, N., Martin-Lauzer, F.R., Moller, D., Murphy, P., Palombi, L., Raimondi, V., Reisser, J., Romero, L., Simis, S.G., Sterckx, S., Thompson, R.C., Topouzelis, K.N., van Sebille, E., Veiga, J.M., and Vethaak, A.D. (2019). Measuring marine plastic debris from space: Initial assessment of observation requirements. Remote Sensing *11*. URL: https://www.mdpi.com/2072-4292/11/20/2443. doi: 10.3390/rs11202443.

12. Schreyers, L., Van Emmerik, T., Biermann, L., and Van Der Ploeg, M. (2022). Direct and indirect river plastic detection from space. In IGARSS 2022 - 2022 IEEE International Geoscience and Remote Sensing Symposium vol. 2022-July. Institute of Electrical and Electronics Engineers Inc. pp. 5539–5542. doi: 10.1109/IGARSS46834.2022.9883379.

13. Simpson, M.D., Marino, A., de Maagt, P., Gandini, E., Hunter, P., Spyrakos, E., Tyler, A., and Telfer, T. (2022). Monitoring of plastic islands in river environment using Sentinel-1 SAR data. Remote Sensing *14*. doi: 10.3390/rs14184473.

14. Garaba, S.P., and Park, Y.J. (2024). Riverine litter monitoring from multispectral fine pixel satellite images. Environmental Advances *15*, 100451. URL: https://www.sciencedirect.com/science/article/pii/S2666765723001096. doi: https://doi.org/10.1016/j.envadv.2023.100451.

15. Mohsen, A., Kiss, T., and Kovács, F. (2023). Machine learning-based detection and mapping of riverine litter utilizing sentinel-2 imagery. Environmental Science and Pollution Research *30*, 67742–67757. URL: https://doi.org/10.1007/s11356-023-27068-0. doi: 10.1007/s11356-023-27068-0.

16. Hurley, R., Braaten, H.F.V., Nizzetto, L., Steindal, E.H., Lin, Y., Clayer, F., van Emmerik, T., Buenaventura, N.T., Eidsvoll, D.P., Økelsrud, A., Norling, M., Adam, H.N., and Olsen, M. (2023). Measuring riverine macroplastic: Methods, harmonisation, and quality control. Water Research *235*. doi: 10.1016/j.watres.2023.119902.

17. Liro, M., Mikuś, P., and Zielonka, A. (2025). Field experiment confirms high macroplastic trapping efficiency of wood jams in a mountain river channel. Scientific Reports *15*, 2933. doi: 10.1038/s41598-025-87147-9.

18. González-Fernández, D., Roebroek, C.T., Laufkötter, C., Cózar, A., and van Emmerik, T.H. (2023). Diverging estimates of river plastic input to the ocean. Nature Reviews Earth and Environment *4*, 424–426. doi: 10.1038/s43017-023-00448-3.

19. Tasseron, P.F., van Emmerik, T.H., Vriend, P., Hauk, R., Alberti, F., Mellink, Y., and van der Ploeg, M. (2024). Defining plastic pollution hotspots. Science of the Total Environment *934*. doi: 10.1016/j.scitotenv.2024.173294.

20. Dersseh, M.G., Melesse, A.M., Tilahun, S.A., Abate, M., and Dagnew, D.C. (2019). Water hyacinth: Review of its impacts on hydrology and ecosystem services-lessons for management of lake tana. In Extreme Hydrology and Climate Variability: Monitoring, Modelling, Adaptation and Mitigation. Elsevier pp. 237–251. doi: 10.1016/B978-0-12-815998-9.00019-1.

21. Villamagna, A.M., and Murphy, B.R. (2010). Ecological and socio-economic impacts of invasive water hyacinth (eichhornia crassipes): A review. Freshwater Biology *55*, 282–298. doi: 10.1111/j.1365-2427.2009.02294.x.

22. Schreyers, L., van Emmerik, T., Nguyen, T.L., Phung, N.A., Kieu-Le, T.C., Castrop, E., Bui, T.K.L., Strady, E., Kosten, S., Biermann, L., van den Berg, S.J., and van der Ploeg, M. (2021). A field guide for monitoring riverine macroplastic entrapment in water hyacinths. Frontiers in Environmental Science *9*. doi: 10.3389/fenvs.2021.716516.

23. Schreyers, L., van Emmerik, T.H., Bui, T.K.L., Biermann, L., Uijlenhoet, R., Nguyen, H.Q., Wallerstein, N., and van der Ploeg, M. (2024). Water hyacinths retain river plastics. Environmental Pollution *356*, 124118. doi: 10.1016/J.ENVPOL.2024.124118.

24. van Emmerik, T.H.M., Janssen, T.W., Jia, T., Bui, T.K.L., Taormina, R., Nguyen, H.Q., and Schreyers, L.J. (2025). Plastic pollution and water hyacinths consistently co-occur in the lower saigon river. Environmental Research: Water *1*, 045001. URL: https://doi.org/10.1088/3033-4942/ae10d7. doi: 10.1088/3033-4942/ae10d7.

25. Janssens, N., Schreyers, L., Biermann, L., Van Der Ploeg, M., Bui, T.K.L., and Van Emmerik, T. (2022). Rivers running green: Water hyacinth invasion monitored from space. Environmental Research Letters *17*. doi: 10.1088/1748-9326/ac52ca.

26. Thamaga, K.H., and Dube, T. (2018). Remote sensing of invasive water hyacinth (eichhornia crassipes): A review on applications and challenges. Remote Sensing Applications: Society and Environment *10*, 36–46. doi: 10.1016/j.rsase.2018.02.005.

27. Schreyers, L., van Emmerik, T., Nguyen, T.L., Castrop, E., Phung, N.A., Kieu-Le, T.C., Strady, E., Biermann, L., and van der Ploeg, M. (2021). Plastic plants: The role of water hyacinths in plastic transport in tropical rivers. Frontiers in Environmental Science *9*. doi: 10.3389/fenvs.2021.686334.

28. van Emmerik, T., Strady, E., Kieu-Le, T.C., Nguyen, L., and Gratiot, N. (2019). Seasonality of riverine macroplastic transport. Scientific Reports *9*. doi: 10.1038/s41598-019-50096-1.

29. Kleinschroth, F., Winton, R.S., Calamita, E., Niggemann, F., Botter, M., Wehrli, B., and Ghazoul, J. (2021). Living with floating vegetation invasions. Ambio *50*, 125–137. doi: 10.1007/s13280-020-01360-6.

30. van Calcar, C.J., and van Emmerik, T.H. (2019). Abundance of plastic debris across european and asian rivers. Environmental Research Letters *14*. doi: 10.1088/1748-9326/ab5468.

31. Schreyers, L.J., Bui, K., van Emmerik, T., Biermann, L., Uijlenhoet, R., Nguyen, H.Q., and van der Ploeg, M.J. (2023). Discontinuity in fluvial plastic transport increased by floating vegetation. ESS Open Archive. doi: 10.22541/essoar.167590832.28978202/v1.

32. Roebroek, C.T., Laufkötter, C., González-Fernández, D., and van Emmerik, T. (2022). The quest for the missing plastics: Large uncertainties in river plastic export into the sea. Environmental Pollution *312*. doi: 10.1016/j.envpol.2022.119948.

33. Redmon, J., Divvala, S., Girshick, R., and Farhadi, A. (2016). You only look once: Unified, real-time object detection. In Proceedings of the IEEE conference on computer vision and pattern recognition. pp. 779–788.

34. Jia, T., Kapelan, Z., de Vries, R., Vriend, P., Peereboom, E.C., Okkerman, I., and Taormina, R. (2023). Deep learning for detecting macroplastic litter in water bodies: A review. Water Research *231*. doi: 10.1016/j.watres.2023.119632.

35. Phetanan, K., Hong, S.M., Yun, D., Lee, J., Chotpantarat, S., Jeong, H., and Cho, K.H. (2024). Enhancing flow rate prediction of the chao phraya river basin using SWAT–LSTM model coupling. Journal of Hydrology: Regional Studies *53*. doi: 10.1016/j.ejrh.2024.101820.

36. Park, E., Lim, J., Ho, H.L., Herrin, J., and Chitwatkulsiri, D. (2021). Source-to-sink sediment fluxes and budget in the chao phraya river, thailand: A multi-scale analysis based on the national dataset. Journal of Hydrology *594*. doi: 10.1016/j.jhydrol.2020.125643.

37. Mani, T., Hawangchu, Y., Khamdahsag, P., Lohwacharin, J., Phihusut, D., Arsiranant, I., Junchompoo, C., and Piemjaiswang, R. (2023). Gaining new insights into macroplastic transport 'hotlines' and fine-scale retention-remobilisation using small floating high-resolution satellite drifters in the chao phraya river estuary of bangkok. Environmental Pollution *320*. doi: 10.1016/j.envpol.2023.121124.

38. Coleman, J., and Huh, O. (2004). Major world deltas : a perspective from space.. Louisiana State University (Baton Rouge, La.). Coastal Studies Institute.

39. Mani, T., Ebner, R., Lebreton, L., Khamdahsag, P., Phihusut, D., Hawangchu, Y., Lohwacharin, J., and Piemjaiswang, R. (2025). The tidal trap — seasonal transport of floating macrodebris in the bi-directional chao phraya river network on the gulf of thailand. Marine Pollution Bulletin *212*. doi: 10.1016/j.marpolbul.2025.117605.

40. Main-Knorn, M., Pflug, B., Louis, J., Debaecker, V., Müller-Wilm, U., and Gascon, F. (2017). Sen2cor for sentinel-2. In Image and signal processing for remote sensing XXIII vol. 10427. SPIE pp. 37–48.

41. The scikit-learn developers (2025). scikit-learn. https://doi.org/10.5281/zenodo.17084288. Zenodo.

42. EO Research Team (2024). eo-learn. https://doi.org/10.5281/zenodo.13847341. Zenodo.

43. Hu, C. (2009). A novel ocean color index to detect floating algae in the global oceans. Remote Sensing of Environment *113*, 2118–2129.

44. Sanchez, A.H., Picoli, M.C.A., Camara, G., Andrade, P.R., Chaves, M.E.D., Lechler, S., Soares, A.R., Marujo, R.F.B., Simões, R.E.O., Ferreira, K.R., and Queiroz, G.R. (2020). Comparison of cloud cover detection algorithms on sentinel–2 images of the amazon tropical forest. Remote Sensing *12*. URL: https://www.mdpi.com/2072-4292/12/8/1284. doi: 10.3390/rs12081284.

45. Cabreira, T.M., Brisolara, L.B., and Ferreira Jr., P.R. (2019). Survey on coverage path planning with unmanned aerial vehicles. Drones *3*. URL: https://www.mdpi.com/2504-446X/3/1/4. doi: 10.3390/drones3010004.

46. Geraeds, M., van Emmerik, T., de Vries, R., and bin Ab Razak, M.S. (2019). Riverine plastic litter monitoring using unmanned aerial vehicles (uavs). Remote Sensing *11*. URL: https://www.mdpi.com/2072-4292/11/17/2045. doi: 10.3390/rs11172045.

47. van Emmerik, T., Janssen, T., Bui, T.K., and Schreyers, L. (2024). Annotated images of floating plastic items and water hyacinths. 4TU.ResearchData. doi: 10.4121/78bb4822-7b70-4632-887a-7cacd344024e.v1.

48. Tkachenko, M., Malyuk, M., Holmanyuk, A., and Liubimov, N. (2020). Label studio: Data labeling software. https://github.com/heartexlabs/label-studio. .

49. Padilla, R., Netto, S.L., and da Silva, E.A.B. (2020). A survey on performance metrics for object-detection algorithms. In 2020 International Conference on Systems, Signals and Image Processing (IWSSIP). pp. 237–242. doi: 10.1109/IWSSIP48289.2020.9145130.

50. Varghese, R., and M., S. (2024). Yolov8: A novel object detection algorithm with enhanced performance and robustness. In 2024 International Conference on Advances in Data Engineering and Intelligent Computing Systems (ADICS). pp. 1–6. doi: 10.1109/ADICS58448.2024.10533619.

51. Andriolo, U., Topouzelis, K., van Emmerik, T.H., Papakonstantinou, A., Monteiro, J.G., Isobe, A., Hidaka, M., Kako, S., Kataoka, T., and Gonçalves, G. (2023). Drones for litter monitoring on coasts and rivers: suitable flight altitude and image resolution. Marine Pollution Bulletin *195*, 115521. doi: 10.1016/j.marpolbul.2023.115521.

52. Harvey, P. (2016). Exiftool. https://exiftool.org/. .

53. Jia, T., Taormina, R., de Vries, R., Kapelan, Z., van Emmerik, T.H., Vriend, P., and Okkerman, I. (2026). A semi-supervised learning-based framework for quantifying litter fluxes in river systems. Water Research *289*, 124833. URL: https://www.sciencedirect.com/science/article/pii/S0043135425017361. doi: https://doi.org/10.1016/j.watres.2025.124833.

54. Iamtrakul, P., Padon, A., and Chayphong, S. (2024). Quantifying the impact of urban growth on urban surface heat islands in the bangkok metropolitan region, thailand. Atmosphere *15*. URL: https://www.mdpi.com/2073-4433/15/1/100. doi: 10.3390/atmos15010100.

55. Petrell, R., and Bagnall, L. (1991). Hydromechanical properties of water hyacinth mats. Aquacultural Engineering *10*, 133–147. URL: https://www.sciencedirect.com/science/article/pii/0144860991900066. doi: https://doi.org/10.1016/0144-8609(91)90006-6.

56. Seehawong, C. (2016). Removal of water hyacinth above chao phraya dam completed. https://www.bangkokpost.com/thailand/general/1058001/removal-of-water-hyacinth-above-chao-phraya-dam-completed. . Bangkok Post.

57. Reddy, K.R., and Sutton, D.L. (1984). Waterhyacinths for water quality improvement and biomass production. Journal of Environmental Quality *13*, 1–8. doi: 10.2134/jeq1984.00472425001300010001x.

58. The Ocean Cleanup (2021). Interceptor 004: The First in the Caribbean — Updates — The Ocean Cleanup — theoceancleanup.com. https://theoceancleanup.com/updates/interceptor-004-the-first-in-the-carribean/. . [Accessed 29-02-2024].

59. Pritasari Arumdati, K. (2021). Hidden Secrets of the Water Hyacinth and the Guardians of the Citarum River - Clean Currents Coalition — cleancurrentscoalition.org. https://cleancurrentscoalition.org/hidden-secrets-of-the-water-hyacinth-and-the-guardians-of-the-citarum-river/. . [Accessed 29-02-2024].

60. van Lieshout, C., van Oeveren, K., van Emmerik, T., and Postma, E. (2020). Automated river plastic monitoring using deep learning and cameras. Earth and Space Science *7*. doi: 10.1029/2019EA000960.

61. Vriend, P., Bosker, T., Mellink, Y., Collas, F., Moscoso Cruz, F., Kamp, N., Drok, S., Vijver, M.G., and van Emmerik, T.H.M. (2025). Uncertainties in visual observations of floating riverine plastic. ACS ES&T Water *5*, 3920–3928. URL: https://doi.org/10.1021/acsestwater.5c00223. doi: 10.1021/acsestwater.5c00223. arXiv:https://doi.org/10.1021/acsestwater.5c00223.

62. Tasseron, P.F., van Emmerik, T.H.M., de Winter, W. et al. (2024). Riverbank plastic distributions and how to sample them. Microplastics and Nanoplastics *4*, 22. URL: https://doi.org/10.1186/s43591-024-00100-x. doi: 10.1186/s43591-024-00100-x.

63. Maathuis, M.I., Rußwurm, M., Bochow, M., and van Emmerik, T.H. (2026). Exploring plastic detectability on riverbanks using remote sensing. Marine Pollution Bulletin *229*, 119751. doi: https://doi.org/10.1016/j.marpolbul.2026.119751.

64. Oliveira Junior, E.S., van Bergen, T.J., Nauta, J., Budiša, A., Aben, R.C., Weideveld, S.T., de Souza, C.A., Muniz, C.C., Roelofs, J., Lamers, L.P. et al. (2021). Water hyacinth's effect on greenhouse gas fluxes: a field study in a wide variety of tropical water bodies. Ecosystems *24*, 988–1004.

65. Otieno, D., Nyaboke, H., Nyamweya, C.S., Odoli, C.O., Aura, C.M., and Outa, N.O. (2022). Water hyacinth (eichhornia crassipes) infestation cycle and interactions with nutrients and aquatic biota in winam gulf (kenya), lake victoria. Lakes & Reservoirs: Research & Management *27*, e12391.

66. Jernelöv, A. (2017). Water hyacinths in africa and asia. In The Long-Term Fate of Invasive Species: Aliens Forever or Integrated Immigrants with Time? pp. 117–136.. Springer pp. 117–136.

67. Hauk, R., van Emmerik, T.H., van der Ploeg, M., De Winter, W., Boonstra, M., Löhr, A.J., and Teuling, A.J. (2023). Macroplastic deposition and flushing in the meuse river following the july 2021 european floods. Environmental Research Letters *18*, 124025.

68. Bansal, M., Santhiya, D., and Sharma, J.G. (2024). Mechanistic understanding on the uptake of micro-nano plastics by plants and its phytoremediation. Environmental Science and Pollution Research *31*, 8354–8368.

69. Yin, J., Zhu, T., Li, X., Wang, F., and Xu, G. (2025). Phytoremediation of microplastics by water hyacinth. Environmental Science and Ecotechnology *24*, 100540. URL: https://www.sciencedirect.com/science/article/pii/S2666498425000183. doi: https://doi.org/10.1016/j.ese.2025.100540.

70. Jia, T. (2024). deep plastic yolov8. https://github.com/TianlongJia/deep_plastic_YoloV8. .

STAR METHODS

Key resources table

Reagent or Resource	Source	Identifier
Deposited data		
UAV imagery	This study	https://doi.org/10.4121/f771da08-8143-4a4b-9ad6-c8e711812a63.v1
Bridge-mounted camera imagery	This study	https://doi.org/10.4121/f771da08-8143-4a4b-9ad6-c8e711812a63.v1
Visual counting	This study	https://doi.org/10.4121/f771da08-8143-4a4b-9ad6-c8e711812a63.v1
Physical sampling	This study	https://doi.org/10.4121/f771da08-8143-4a4b-9ad6-c8e711812a63.v1
Ground truth annotations	This study	https://doi.org/10.4121/f771da08-8143-4a4b-9ad6-c8e711812a63.v1
Software and algorithms		
Python v3.8.10	Python Software Foundation	https://www.python.org
scikit-learn	Python Software Foundation	https://scikit-learn.org/
eo-learn	eo research team	https://eo-learn.readthedocs.io/
YOLOv8	Ultralytics	https://github.com/ultralytics/ultralytics
YOLOv8 models	Ultralytics	https://github.com/TianlongJia/deep_plastic_YoloV8
LabelStudio	Tkachenko et al., 2020	https://labelstud.io/
ExifTool	Harvey, 2016	https://exiftool.org/
Water hyacinth classification tool (Sentinel-2)	This study	https://github.com/GielHagenbeek/Waterhyacinth_classification_Sentinel2
Google Colab	Google	https://colab.research.google.com/
Other		
Sentinel-2 imagery	Copernicus Program	https://sentinels.copernicus.eu/

Method details

Overall Methodology

This study integrated satellite remote sensing, UAV and bridge-mounted imaging, visual observations, and physical sampling to quantify water hyacinth (WH) coverage, floating plastic trans-

port, and plastic–hyacinth interactions. Sentinel-2 imagery was used for WH classification from space, and object detection was applied for WHs and plastics in UAV and bridge imagery.

Study Area

The study covered a 62.1 km stretch of the lower Chao Phraya River (Thailand), from 104.5 to 42.4 km upstream of the Gulf of Thailand. This tidal-influenced section experiences strong seasonal discharge variability and is a major transport corridor through the Bangkok Metropolitan Area. Images were collected over eight cross-sections of the river width.

Bridge-mounted camera imagery

Bridge-mounted imagery was collected at four locations (B1–B4) during four sampling periods using a GoPro Hero 11 mounted on a 1 m arm to capture nadir images of the river surface. Five waypoints per bridge were distributed across the river width and revisited in multiple rounds per date, with images captured at 10-second intervals. Camera placement and field of view were configured to avoid riverbanks and bridge structures. In total, 14,742 images were acquired and used, with camera height measurements incorporated to calculate ground sampling distance.

UAV Imagery

UAV imagery was collected at four river cross-sections on two dates using a DJI Mavic 3 Enterprise equipped with an RGB camera. Flights followed a perpendicular crossing pattern across the river, with repeated crossings conducted in morning and afternoon sessions to account for tidal conditions. Flight height and crossing frequency varied due to operational constraints, including battery life and river width. After filtering riverbank images, 6,402 UAV images were retained for analysis

Visual Counting

Floating plastics were counted at each waypoint over $\sim$5 min, noting free-floating vs. entangled in WHs and classified into eight plastic types. High-flow events were estimated by grouping items or shortening counts. Surface transport rates and trapping ratios were calculated per waypoint and averaged to represent each river date and location.

Physical Sampling

WH patches were collected (1–4 Apr) and weighed on board. Entangled plastics $\geq$ 0.5 cm in any direction were categorized and counted. On shore, a subset of all plastics was weighed to estimate mean mass per plastic category.

Sentinel-2 Data and Application

Cloud-filtered Sentinel-2 images (10–20 m; June 2024–June 2025) were used to estimate WH coverage across four study segments. A pre-trained Naive Bayes classifier (using NDVI, FAI, B2, B3, B12) was applied to SCL-validated non-cloudy pixels. WH-classified pixels were aggregated per segment and expressed as percentage river-area coverage.

Object Detection Data and Application

High-resolution imagery consisted of UAV data collected by DJI Mavic 3 Enterprise (four sites) and bridge-mounted GoPro Hero 11 imagery (four sites) along the 62-km study reach. Images were captured in nadir orientation. YOLOv8 models (*HyacinthModel* and *PlasticModel*) were applied to tiled or resized images to detect WHs, free-floating plastics, and plastics entangled in WH patches. Detections were converted to surface area using ground-sampling distance based on flight altitude and camera height.

Model Performance Evaluation

A validation set of 82 images (70% GoPro, 30% UAV) from 21,144 total images was annotated (1,415 objects; 54% GoPro, 46% UAV) using LabelStudio. Annotations were tiled for the PlasticModel. Class distributions were kept balanced, and bounding boxes were recalculated to original image sizes. Model performance was assessed using YOLOv8 metrics: precision, recall, mAP50, and mAP50–95 at a confidence threshold of 0.5.

Model Output Settings

Predictions were compared with ground truth annotations using Intersection over Union (IoU $\geq$

0.5) to define True Positives, False Positives, and False Negatives. Confidence thresholds (0.00–1.00, step 0.05) were tested, and the optimal threshold for each model was selected based on the highest F1-score. For the PlasticModel, thresholds for free-floating plastics were applied.

Quantification and statistical analysis

Statistical details of experiments, including the number of observations (n) can be found in the figures, tables, Results and Methods sections. Spearman's rank correlation was used to test relationships between relevant metrics. Correlations were calculated on mean values per location, with statistical significance defined at $p < 0.05$. Correlation coefficients (r) and associated p-values were also reported to assess linear relationships where applicable. No data points were excluded. All statistical parameters, including per-class F1-scores are reported alongside figures, tables, and in the Results section. No randomization or blinding was applied, as the study relied on deterministic classification and observational measurements.